USGS-OFR-87-409

USGS-OFR-87-409

UNITED STATES
DEPARTMENT OF THE INTERIOR
GEOLOGICAL SURVEY

PHOTOGEOLOGIC STUDY OF SMALL-SCALE LINEAR FEATURES NEAR A POTENTIAL NUCLEAR-WASTE REPOSITORY SITE AT YUCCA MOUNTAIN, SOUTHERN NYE COUNTY, NEVADA

By

C. K. THROCKMORTON

Open-File Report 87-409

Prepared in cooperation with the
Nevada Operations Office
U.S. Department of Energy
(Interagency Agreement DE-AI08-78ET44802)

Denver, Colorado
1987

 USGS-OFR-87-409

UNITED STATES DEPARTMENT OF THE INTERIOR

GEOLOGICAL SURVEY

PHOTOGEOLOGIC STUDY OF SMALL-SCALE LINEAR FEATURES NEAR A POTENTIAL NUCLEAR-WASTE REPOSITORY SITE AT YUCCA MOUNTAIN, SOUTHERN NYE COUNTY, NEVADA

By

C. K. Throckmorton[1/]

1/U.S. Geological Survey, Denver, Colorado

CONTENTS

ILLUSTRATIONS

TABLES

PHOTOGEOLOGIC STUDY OF SMALL-SCALE LINEAR FEATURES NEAR A POTENTIAL NUCLEAR-WASTE REPOSITORY SITE AT YUCCA MOUNTAIN, SOUTHERN NYE COUNTY, NEVADA

By

C. K. Throckmorton

ABSTRACT

Linear features were mapped from 1:2400-scale aerial photographs of the northern half of the potential underground nuclear-waste repository site at Yucca Mountain by means of a Kern PG 2 stereoplotter. These features were thought to be the expression of fractures at the ground surface (fracture traces), and were mapped in the caprock, upper lithophysal, undifferentiated lower lithophysal and hackly units of the Tiva Canyon Member of the Miocene Paintbrush Tuff. In order to determine if the linear features corresponded to fracture traces observed in the field, stations (areas) were selected on the map where the traces were both abundant and located solely within one unit. These areas were visited in the field, where fracture-trace bearings and fracture-trace lengths were recorded. Additional data on fracture-trace length and fracture abundance, obtained from ground-based studies of cleared pavements located within the study area (Barton and Larsen, 1985, Christopher C. Barton and others, USGS, written commun., 1985) were used to help evaluate data collected for this study.

Bearings of traces measured from the photogeologic map are dissimilar to bearings of fracture traces recorded in the field. Groups of trace orientations recognized in the field are missing or are poorly represented in their photo counterparts. Also, for all stations, the number of photogeologic traces mapped (all greater than 3.2 m long) exceeds the number of fractures greater than 3 m long observed in the field, suggesting that many photogeologic traces are erroneous. Field work confirmed that the photogeologic map includes linear features first thought to be fracture traces, but that cannot be related to fracture traces observed in the field.

The 1:2400 photographic scale, although large, nevertheless was not adequate to discern the majority of fracture traces observed in the field. This factor, coupled with incomplete bedrock exposures resulted in more than 66-87 percent of the fractures remaining undetected. Thus, traces recorded on the photogeologic map do not accurately characterize the fracture patterns in the units studied. Yucca Mountain is poorly suited to this type of study.

INTRODUCTION

This report presents the results of an aerial photographic study of part of the northern half of Yucca Mountain, the site of a potential underground repository for high-level radioactive waste, adjacent to the Nevada Test Site in southern Nevada (figs. 1 and 2). The study was undertaken in connection with the U.S. Department of Energy, Nevada Nuclear Waste Storage Investigations (NNWSI) (Interagency Agreement DE-AI08-78ET44802) as part of a

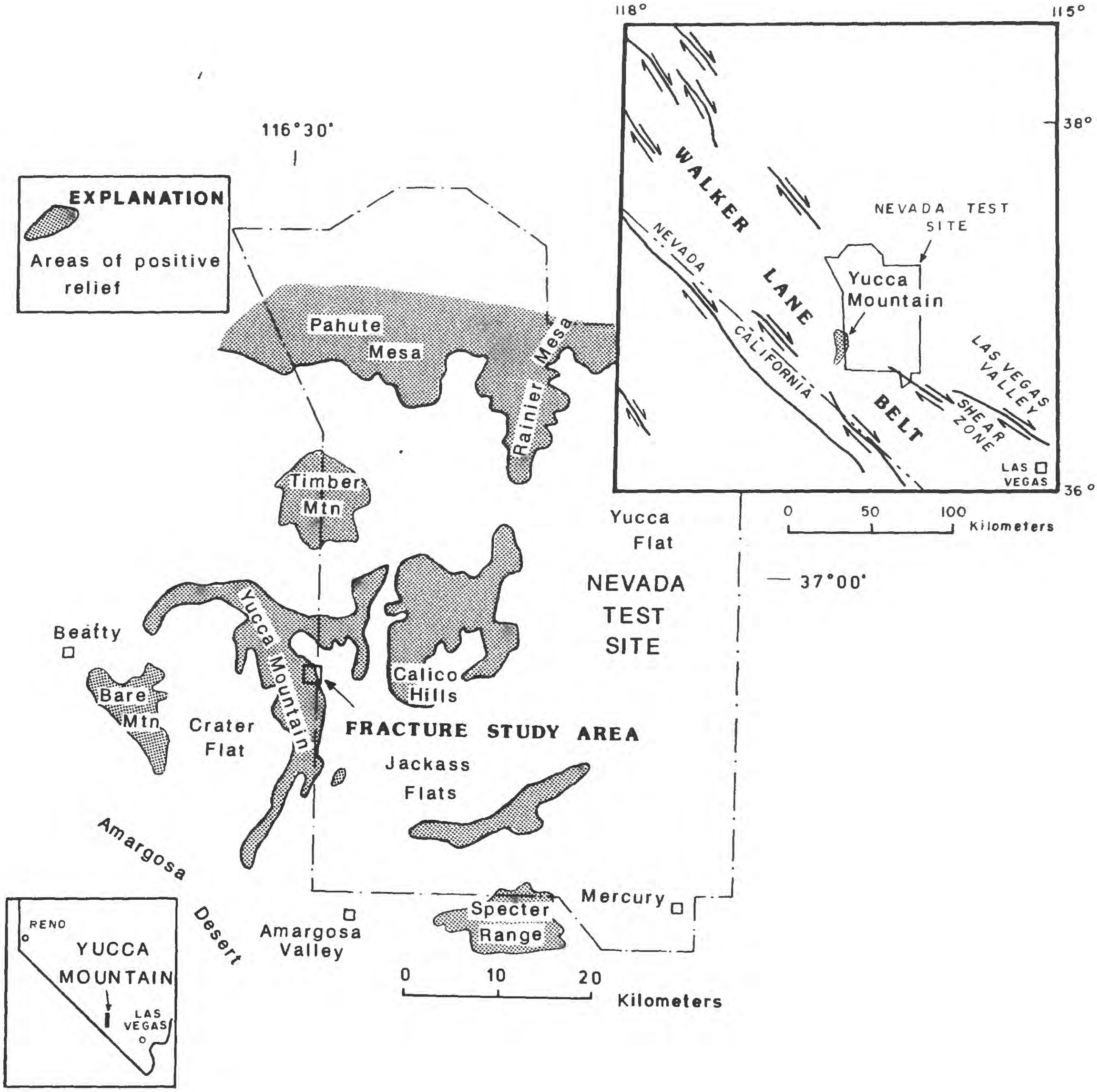

Figure 1.--Location map of Yucca Mountain and the Nevada Test Site showing regional setting of Yucca Mountain. Major zones of right-lateral strike-slip faulting in the Walker Lane and Las Vegas Valley shear zones are from Carr (1974) and Stewart and Carlson (1978).

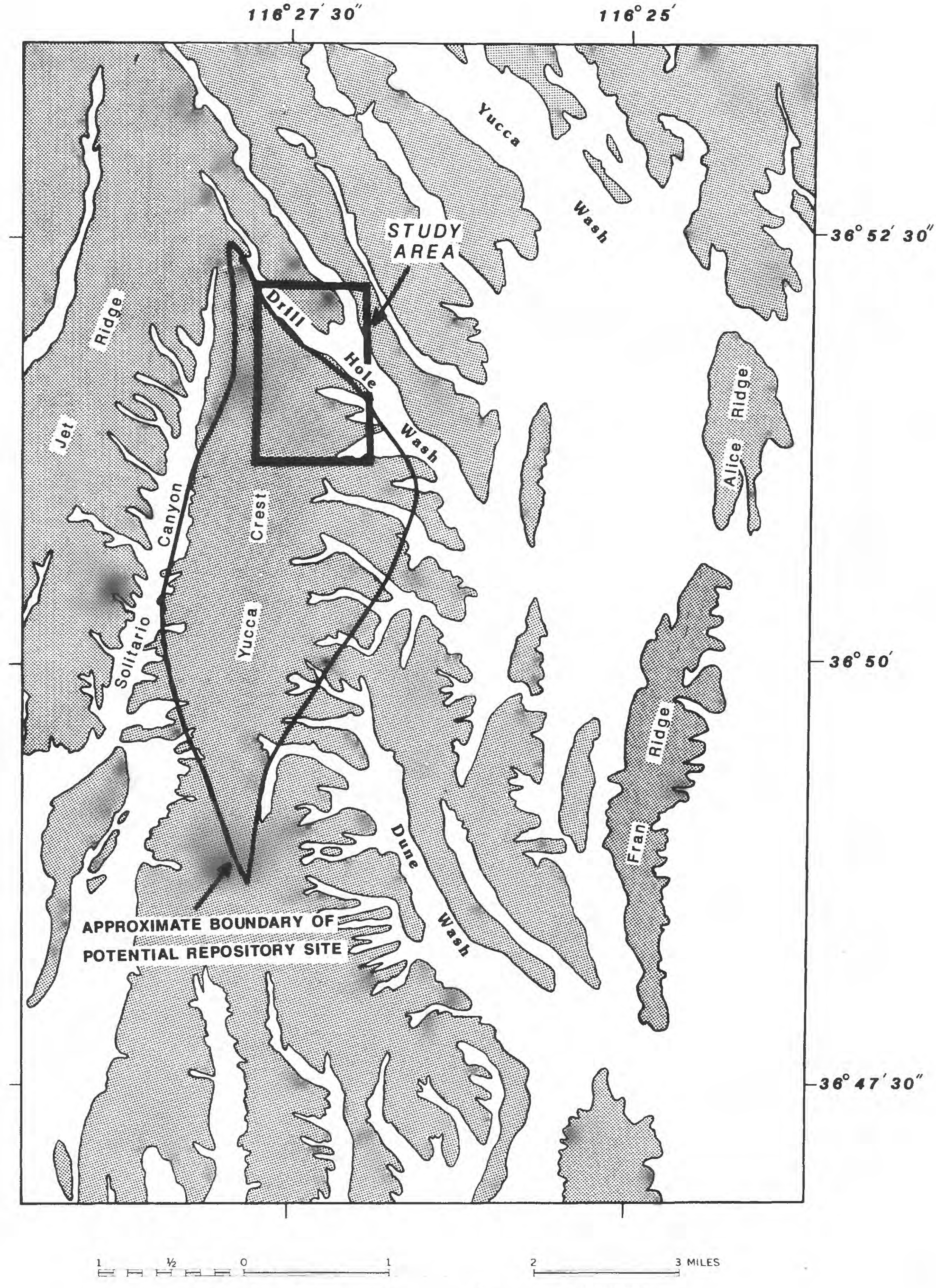

Figure 2.--Yucca Mountain showing the location of the study area and the potential repository site.

larger effort by the U.S. Geological Survey (USGS) to characterize fractures at Yucca Mountain. Aerial photographs provide the potential for total, continuous coverage of an area so that isolated field stations can be related one to another. The linear features visible on the photographs were thought to be fracture traces. One objective of this study was to evaluate the suitability of photogeologic mapping for documenting local fracture patterns and for determining the degree of variation among the patterns. Another objective was to ascertain how well the bearings of linear features obtained from the aerial photographs agree with fracture strikes recorded from ground-based studies of cleared pavements (Barton and Larsen, 1985), and whether the photo data could be used to interpolate between those pavements. Comparison of patterns mapped from aerial photographs with the actual fracture network documented in the field was used to evaluate the utility of photogeologic mapping of fractures.

GEOLOGIC SETTING

The Nevada Test Site and Yucca Mountain are in southern Nevada, on the southeastern margin of the physiographic Great Basin subprovince (Synder and others, 1964). Yucca Mountain is a Tertiary volcanic highland located between right-lateral strike-slip faults of the Walker Lane Belt and Las Vegas Valley shear zones (fig. 1). The Walker Lane Belt is characterized by low-relief hills and desert valleys constructed by transcurrent faulting as opposed to the more typical normal faulting of the Great Basin. Yucca Mountain consists of a series of north-trending, eastward-dipping, elongate fault blocks bounded by steeply dipping Basin-and-Range style normal faults. At Yucca Mountain, north to north-northeast-striking Basin-and-Range faults have been recognized (Scott and Bonk, 1984). The northern end of Yucca Mountain is thought to be cut by a number of right-lateral northwest-striking faults (Scott and Bonk, 1984). These faults may be related to the Las Vegas Valley shear zone and the Walker Lane deformation (Scott and others, 1984). Swarms of steeply dipping normal faults each with small offsets (normally less than 10 meters) are common in the southern half of the mountain (Scott and Bonk, 1984), while the central part is relatively unfaulted (Scott and others, 1984).

Yucca Mountain is a dissected plateau consisting of prominent north-trending ridges as much as 700 m above adjacent steep-sided ravines and washes. The summit surfaces are relatively flat, ranging in altitude from about 1200 to 1800 m.

Yucca Mountain is composed of Miocene volcanic ash-flow and ash-fall tuffs erupted from the Claim Canyon caldera 2 km to the north, and is underlain at a depth of about 1-2 km by Paleozoic marine clastic rocks and Mesozoic granitic intrusions (Snyder and Carr, 1982). Only the Tiva Canyon Member of the Paintbrush Tuff is exposed within the study area. Scott and Bonk (1984) have divided this member into several informal units at Yucca Mountain which are in ascending order: columnar, hackly, lower lithophysal, rounded step, upper lithophysal, upper cliff, and caprock. The complete volcanic stratigraphic section is given in Scott and Bonk, 1984. Christopher C. Barton and others (USGS, written commun., 1985) have remapped the volcanic section on Live Yucca Ridge, retaining the units defined and described by Scott and Bonk (1984).

CLIMATE AND VEGETATION

The Nevada Test Site is a semiarid desert. Mean annual temperature is 15 °C and mean annual precipitation is 117 mm (Emily M. Taylor, USGS, written commun., 1986). Two storm types exist in the study area, resulting in precipitation derived from (1) winter cyclonic activity, and (2) intense summer convection (Houghton and others, 1975). This seasonal variation in precipitation influences soil properties which, in turn, influence both type and distribution of vegetation (Emily M. Taylor, USGS, written commun., 1986).

Topography, geology, and local climates at the Nevada Test Site exert a strong influence on vegetation, resulting in a complex mosaic of plant associations (Spaulding, 1985). Principal plant-community types at Yucca Mountain are varieties of the Great Basin desertscrub and Mojave desertscrub communities (Spaulding, 1985; classification from Brown and others, 1979) and the transition desert community (Beatley, 1976). At Yucca Mountain, species representative of the Great Basin desertscrub community generally occur at elevations from about 1500 to 2000 m, while those of the transition desert and Mojave desertscrub community generally occur at elevations below 1200 m (Spaulding, 1985). The ridgetops and slopes are represented by a well-mixed community including *Lycium andersonii*, *Ceratoides lanata*, *Atriplex canescens*, and several species of *Ephedra*. Mojave desertscrub shrubs like creosote bush (*Larrea divaricata*) and white bursage (*Ambrosa dumosa*) are common at lower elevations in washes and ravines.

METHOD OF STUDY

Evaluation of Methods and Materials

The study began with an evaluation of existing sets of aerial photographs, topographic base maps, and instruments for stereographic viewing of the photographs, in order to select the materials and methods best suited for this study. A Topcon table mirror stereoscope and a Kern PG 2 photogrammetric plotting instrument were available for viewing the photographs. Linear features were mapped from test photographs using both instruments to determine which would provide the most accurate information in the most efficient manner.

The mirror stereoscope has a built-in magnifier of 1.8x and accessory 3x binocular eyepieces. In addition, it is equipped with a track attachment, permitting the viewer to examine a wide area without making time-consuming adjustments. Linear features on the aerial photographs were drawn onto a transparent overlay placed over one photograph from each stereo pair.

The Kern plotter is a high-precision optical mechanical plotter with magnification capability of 2x, 4x, and 8x. Features observed in the stereoscopic image are plotted directly onto a base sheet by means of a pantograph that transfers to the base map the same line drawn by the observer in the image. The Kern plotter with the SSL pantograph has an enlargement capability of about 5x to 0.5x. The base sheet scale must be within the limitations of the pantograph. Thus, using 1:2400 aerial photographs restricts the base map to 1:4800, the maximum reduction capability of the Kern plotter.

The Kern plotter was chosen for this study because it has numerous advantages over the table mirror stereoscope. The most important factor is that the high-precision of the Kern plotter assures both accurate and efficient compilation of the geologic data directly onto the base map. In contrast, additional steps are required to transfer data to a base map by the mirror stereoscope method. The aerial photographs can be viewed under a higher magnification (8x) than is possible with the mirror stereoscope, permitting more linear features to be discerned. Differences in scale, and differences in the amounts of tilt and overlap between consecutive photographs required frequent readjustments in order to move from one direction to the next when viewed under the mirror stereoscope. Once each model is oriented on the Kern plotter, however, no further adjustments are necessary.

Paper prints from nine sets of aerial photographs, at scales ranging from 1:1000 to 1:24,000, were evaluated on the basis of several criteria: (1) good tonal quality and resolution; (2) sufficient overlap to allow stereoscopic viewing; (3) sufficiently large scale that linear features could be discerned using the Kern plotter; and (4) areal coverage of at least one-half of the potential Yucca Mountain repository site.

Preliminary mapping of linear features from one stereo pair from each set of photographs revealed considerable variation in quality with regard to resolution, contrast, and tone of the photographs. Also noted were variations in the amount of overlap, differences in scale, and differences in the degree of tilt from consecutive prints within the same set.

Linear features, discernible as fracture traces, were poorly visible on stereo pairs of photographs with scales of 1:7400 or smaller, even when viewed under the highest magnification on the Kern plotter. Primarily, discontinuous alignments of vegetation, some of which follow fracture traces, were visible on the smaller-scale photographs. The largest-scale photographs (1:1000) provided the best view of linear features, but unequal scales and major differences in amount of overlap and degree of tilt between consecutive photographs prevented most of them from being viewed stereoscopically. In addition, this set did not meet the areal coverage requirement. Only the 1:2400 scale photo set met all the criteria listed above, and was thus chosen for study.

Mapping was done under 8x magnification, the maximum available, because linear features were most readily seen when viewed at this magnification.

Two topographic base maps covering most of Yucca Mountain were available at the onset of the study. One, published in 1961 by the U.S. Geological Survey at a scale of 1:24,000, has a contour interval of 20 ft. The alternative was a recently prepared computer-generated base map (Wu, 1985) in six sheets at a scale of 1:5000, with a 2-m contour interval. The computer-generated topographic base map was chosen for this study primarily because of its higher degree of accuracy. An enlargement from 1:5000 to 1:4800 was required to make the base map scale compatible with the 1:2400 photographs and Kern plotter.

Factors Limiting the Area Mapped

Vegetation, soil, and colluvial cover inhibited visibility of linear features on the aerial photographs. At Yucca Mountain, there is greater than 10 percent perennial plant cover (Emily M. Taylor, USGS, written commun., 1986). Vegetation is more abundant on north-facing slopes than south-facing slopes or ridge crests. Ridges with narrow crests have a thin cover of colluvium, while the broad ridge of Yucca Crest and most of the slopes are covered by a thicker talus and colluvium that obscures much of the bedrock. Thus, linear features on the aerial photographs were visible primarily on narrow ridge crests, less frequently on south-facing slopes, and rarely on north-facing slopes.

A preliminary field survey affirmed that although vegetation alignments follow fracture traces, they also follow subunit boundaries, boundaries of talus buildup, and surficial erosional features. Vegetation alignments thus could not be used to map fracture traces from the photos with a usably high degree of confidence.

In the stereo model, vertical exaggeration--the exaggeration of vertical distances with respect to horizontal distances--make the slopes appear much steeper than they are, thereby reducing visibility of linear features on the slopes. These factors restricted the effective area of study to primarily the ridge crests.

Criteria for Photogeologic Mapping of Linear Features

Criteria used to map the linear features were influenced by three factors: (1) the types of features visible on the aerial photographs, (2) the magnification required to see the features, and (3) landforms on which the features were visible. As discussed above, linear features were visible primarily on ridge crests and less frequently on south-facing slopes.

Figure 3 shows a portion of the photogeologic map of linear features superimposed on a topographic map (Wu, 1985) of the study area. Linear features were plotted onto the base sheet, regardless of length. Because the Kern plotter limits the amount of reduction or enlargement with respect to photo and base map scales, many linear features, although visible on the photographs, were not of sufficient length to be measurable on the 1:4800 base map, and were not analyzed. A measurable length of a linear feature on the 1:4800 base map was determined to be a minimum of about 0.7 mm, corresponding to a trace 3.2 m long on the ground surface. In adhering to this criterion, many linear features were eliminated because they were too short to be measured when plotted onto the base map.

The type of linear features visible on the aerial photographs varied when the 1:2400 photographs were viewed at different magnifications. Mostly vegetation alignments and only a few fracture traces were seen under 2x and 4x magnification. On Yucca Crest, only vegetation alignments could be seen at these magnifications.

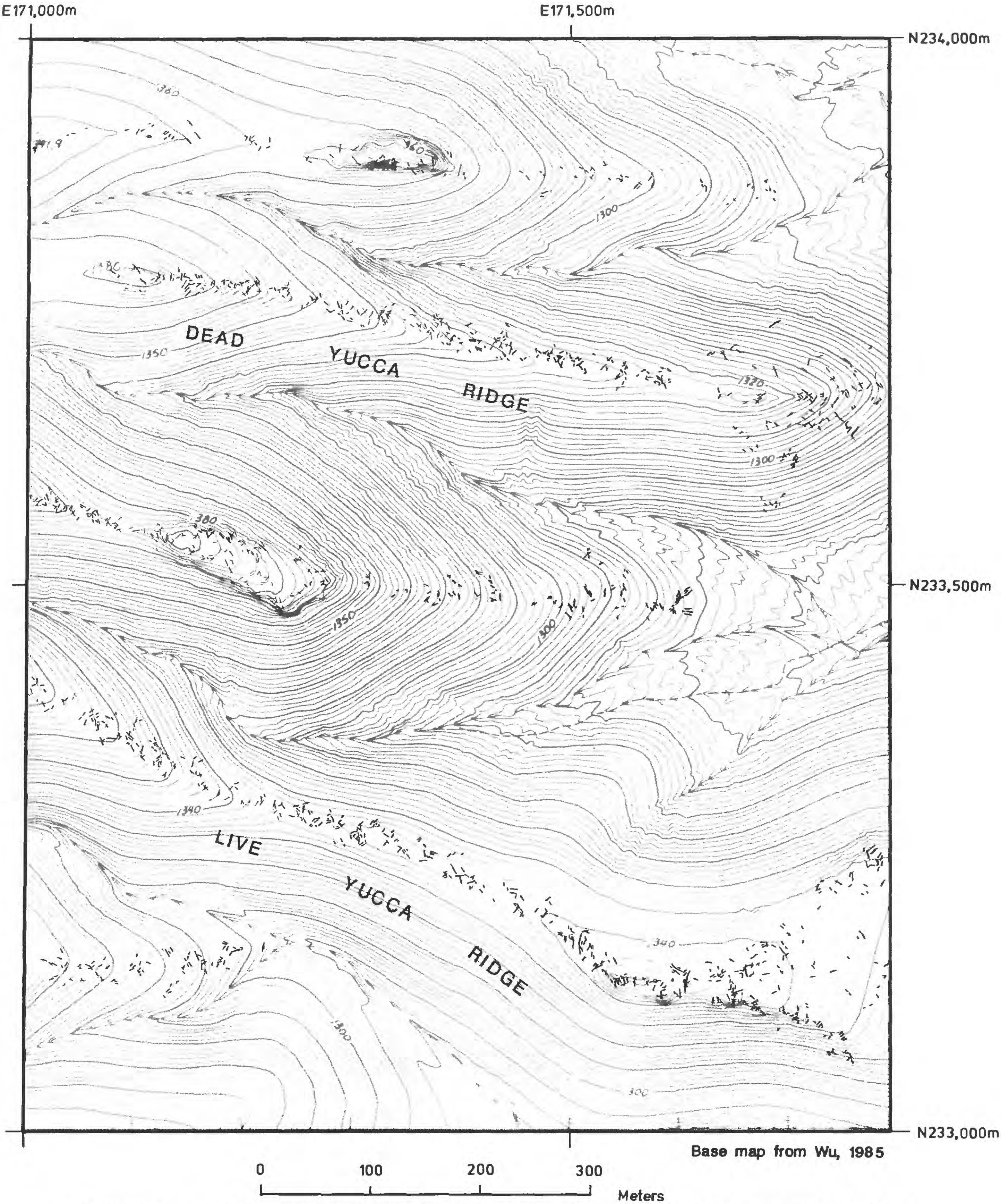

Figure 3.--Portion of photogeologic map showing linear features mapped from aerial photographs.

Except for Yucca Crest, at 8x magnification most linear features were discernible on the photographs as fracture traces. Vegetation alignments were rarely discernible. Fracture traces were particularly conspicuous in the caprock unit on narrow ridge crests where vegetation is sparse and fractures have widened due to lack of constriction along the edges of ridges. With the exception of Yucca Crest, only those linear features discernible as fracture traces were mapped. These fracture traces are seen on the photographs as straight or gently curving lines denoting a parting in the rock. Commonly, bedrock on one side of a fracture was eroded and the vertical or near vertical fracture face and fracture aperture were also visible. The faces were seen on the photographs as shadows, appearing darker than the ground surface.

In the caprock unit on Yucca Crest, however, most of the linear features were visible as thin, faint lines, sometimes associated with vegetation alignments, but more often isolated from vegetation. These features were thought to be fracture traces covered by a thin veneer of soil or talus. In addition, a few fracture traces (with visible aperture and fracture face) were observed. Both types of features were mapped from the photos on Yucca Crest. When stations on Yucca Crest (stations 24 and 52) were visited in the field, none of the faint lines were discernible. Most of the exposed fractures were edges of large blocks of rock which have broken away and moved from their original position. These fractures are interpreted to be the result of surficial erosion, based on criteria discussed in the next section.

In all cases, vegetation alignments were not mapped. However, fracture traces locally were visible between widely spaced aligned shrubs; these traces were inferred to continue through the area covered by the shrubs and were mapped as one continuous trace. Linear features defined by abrupt tonal contrast between adjacent areas on the photographs were rarely observed, and only on Yucca Crest. On the photographs these areas appeared to reflect differences in vegetation types. Visits to these areas confirmed this observation. Other linear features commonly seen on aerial photographs such as textural differences and drainage and soil patterns were not observed on the photographs.

Methods for Field Verification of Photogeologic Map

Linear features within approximately one-third of the study area were mapped from the aerial photographs and their bearings measured with a protractor. Field work was then initiated to determine if the linear features correspond to fracture traces observed in the field. A preliminary ground survey demonstrated that it generally was not possible to identify which fracture trace on the ground corresponded to a specific linear feature on the photos. There are two reasons why this was not possible: (1) an abundance of fracture traces on the ground with similar bearings, and (2) a lack of distinctive topographic features to allow precise location of photogeologic traces on the ground surface. Because individual photogeologic traces were not directly locatable on the ground, another approach was used.

Nine areas (stations) of abundant linear features were delineated on the photogeologic map and subsequently studied in the field. Each station is located solely within one unit of the Tiva Canyon Member of the Paintbrush Tuff. Five stations are located in the caprock unit, three in the upper lithophysal unit, and one in the undifferentiated lower lithophysal and hackly unit. Figure 4 shows the location of each station. All field stations are located in areas where the bedrock is incompletely exposed. The areas encompassed by the stations vary from approximately 153 m^2 to 1244 m^2.

In order to gather field data consistent with fracture data from other studies at Yucca Mountain, the field procedures used in this study follow as closely as possible the procedures adopted by Christopher C. Barton and others (USGS, written commun., 1985) for their fracture outcrop studies of natural pavements. Natural pavements are areas where the bedrock is exposed or covered only by a thin soil or talus. The pavements were cleared of overlying debris to expose the complete fracture network prior to their study. Figure 4 shows the location of the pavements.

The field procedures used in this study are described below; deviations from the procedures of Barton and others are noted.

1. The stations were located in the field using triangulation with a Brunton compass and in some places, by identifying distinct patterns of vegetation on the photographs, and locating these patterns on the ground. Boundaries of stations were staked. The size and shape of each station were determined by selecting areas of abundant traces on the photogeologic map. Each station was traversed by starting at a boundary marker and moving in approximately a 4-m-wide band along the boundary line to the next boundary marker, then back in the opposite direction covering an adjacent 4-m-wide area. This procedure was repeated until the entire area was covered. Traversing the area in this manner ensured measuring a fracture trace only once.
2. All fracture traces longer than 0.3 m were recorded. Each fracture trace was assigned a number, and its orientation (bearing and dip) was measured with a Brunton compass. The bearing measurements are accurate to within $\pm 2°$. Bearing measurements were taken at waist level due to magnetization of some rocks in the study area. When fracture traces were observed to curve, an average of the curve was measured. All fracture traces were observed to curve less than 15° over the exposed trace length.
3. Fractures believed to be of surficial origin were not measured. The recognition of fractures resulting from surficial weathering is somewhat subjective, and criteria used to recognize these fractures do not apply to every fracture. Fractures were interpreted to be caused by surficial weathering based on one or more of the following criteria. (1) The fracture has a short, irregular trace length and propagates only a few centimeters downward. (2) The fracture surface is fresh relative to other fractures in the area. (3) The fracture surface is the edge of an isolated block of bedrock. (4) The fracture is shallow-dipping (less than 30°) and appears to be the result of exfoliation jointing. (5) The fracture aperture is very small (faint crack) and does not appear to have widened from erosion and weathering.
4. Exposed trace lengths were estimated visually for each fracture and assigned to one of three arbitrary length categories: Category 1--length over 3 m, Category 2--length 1-3 m, Category 3--length less than 1 m.

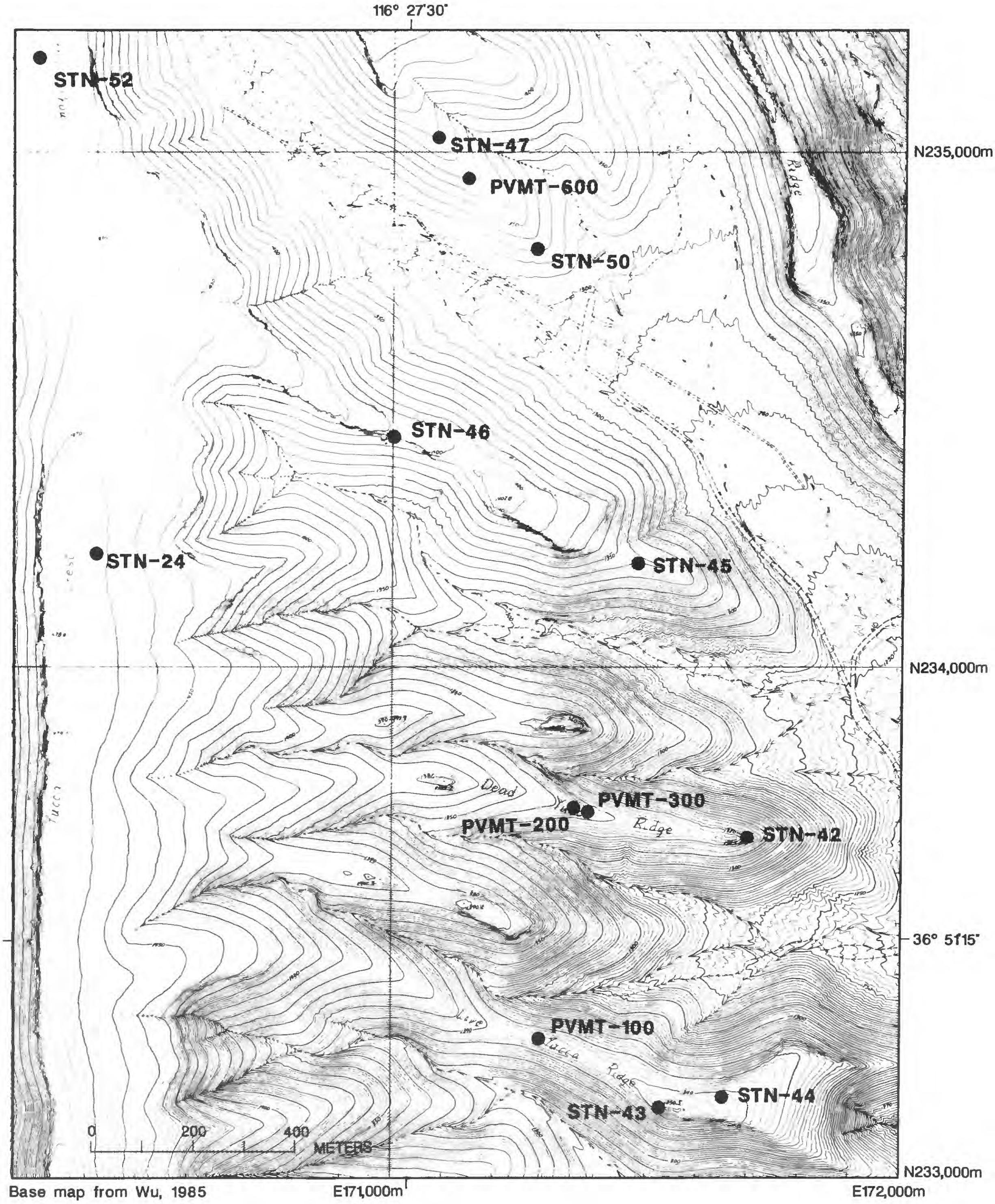

Figure 4.--Map of the study area showing locations of stations and cleared pavements (see figure 2 for location).

5. The surface roughness of each fracture was measured using a contour gage pressed against a portion of the fracture surface, placed for consistency parallel to the fracture strike. Measurements of roughness profiles taken radially on the fracture surface have demonstrated no measurable difference in the surface roughness (Christopher C. Barton, USGS, oral commun., 1986). Tubular structures, identified on cooling joints (Barton and others, 1984) and lithophysal cavities on fracture surfaces were avoided when the surface roughness was measured. A minimum impression length of 10 cm was taken. If less than 10 cm of surface was continuously exposed, a composite was taken from different areas on the fracture surface to equal a minimum length of 10 cm. The roughness profiles can be compared with a standard set of profiles to determine fracture roughness coefficients (FRC), which range from 0-20 (see fig. 8 in Barton and Choubey, 1977). FRC values were not determined for the profiles measured in this study because the FRC's are not germane to the evaluation of the photogeologic map.
6. Also noted, if present, were fracture swarming, abutting relationships, curvature, offsets, presence of tubular structures, mineral-fillings or coatings, surface structures on fracture faces, fractures which cut lithophysae, and degree of weathering of the fracture surface.

Field procedures utilized in this study differ from those of Barton and others (USGS, written commun., 1985) in the following aspects.

1. Barton and others selected natural pavements for their fracture studies. The size of each pavement was determined by the scale of the fracture pattern and the thickness of debris cover. The pavements were cleared of debris prior to study. In this study, stations were preselected by identifying areas on the photogeologic map where linear features were abundant and occurred solely within one geologic unit. The station size was determined by clusters of linear features on the photogeologic map.
2. In this study, only those fractures that had an exposed trace length greater than 0.3 m were measured. Barton and others measured all fractures having exposed trace lengths greater than 0.2 m. In addition, they measured trace lengths directly from approximately 1:50-scale aerial photographs taken from a helicopter.
3. Barton and others measured strikes of fractures exposed on the pavement surfaces. Bearings of fracture traces, not strikes of fractures, were measured in this study in order to compare field data with bearings of fracture traces measured from the photogeologic map. Because of the nearly horizontal pavement and outcrop surfaces, and the steeply-dipping nature of the fractures exposed on the pavement and outcrop surfaces, the measurements, though not identical, are similar enough to be comparable.

DATA ANALYSIS

Bearings of 164 linear features were measured from nine stations on the photogeologic map; 444 fracture-trace bearings were measured at field stations. Orientations, numbers of fractures, and trace lengths from both data sets were analyzed to determine whether the actual fracture pattern can be characterized from the photogeologic map. Trace length and abundance data, obtained from cleared pavements in the upper lithophysal unit of the Tiva Canyon Member (Barton and Larsen, 1985; Christopher C. Barton and others, USGS, written commun., 1985) were used to help evaluate data collected in this study. Data from each unit were treated separately to show the influence of lithology on the fracture patterns. Data collected in the field are hereafter referred to as field data; data obtained from the aerial photos are hereafter referred to as photo data.

Bearings of fracture traces measured at field stations were evaluated with bearings measured from photogeologic traces by means of bearing-distribution histograms. Field and aerial-photo trace-distribution histograms from station 52, located in the caprock unit on Yucca Crest could not be compared because no fractures were observed in the field at this station. Field and photo data from station 24, in the same unit, were also not analyzed due to the low numbers of fractures (five) observed at this field station.

At stations 42, 45 and 47, all located within the upper lithophysal unit, cooling joints were identified in the field based on the presence of tubular structures on joint surfaces. Separate histograms were constructed for these joints (a subset of total fractures measured at each field station), to allow a comparison of joint-trace bearing distributions with joint-strike distributions recorded from pavements by Christopher C. Barton and others (USGS, written commun., 1985).

Trace Orientations

With one exception (station 46), distributions of trace bearings from field plots and photo plots of total traces exhibit no well-defined groups (Appendix III). Field station plot for station 46, located within the caprock unit, shows a group ranging from 325° to 359° that is not apparent in the corresponding aerial-photo plot. Field plots for stations 42, 45, 50, 43, and 46, show some preferred orientation, but bearing distributions are characterized only by broadly clustered groups, and again these distributions do not agree with those plotted from the aerial-photo data. For each station, trace orientations from the two data sets do not agree.

The cooling joint bearings measured in the field appear to form two groups. A northwest-trending group and a northeast-trending group are distinguishable at stations 42, 45, and 47, all located within the upper lithophysal unit. At field station 42, one group of 13 joints ranges from 20° to 40° and the other group (only 2 joints) from 300° to 304°. Joint groups at field station 45 range from 18° to 45° (14 joints) and 310° to 350° (11 joints). Field station 47 exhibits joint groups ranging from 15° to 47° (3 joints) and 331° to 348° (6 joints). It should be noted, however, that the groups are based on very low numbers of cooling joints identified at each field station, and are probably too low to confirm the groups at each locality.

Appendix III shows the combined orientation data from cooling joints identified from field stations in this study and from the cleared pavements. Orientations of joint groups identified in this study are similar to those of cooling-joint sets identified from pavements 100, 200, and 300 of Christopher C. Barton and others (USGS, written commun., 1985), where the sets (based on 128 joints) range from 21° to 60° and 310° to 359°. One cooling-joint set identified from pavement 600 falls within the 21°-60° range (based on 6 joints), except for three joints which fall outside of the range. Identification of joint groups at field stations in this study which are similar to joint sets found on the pavements, suggests that joint sets may be characterized from incompletely exposed outcrops, even when low numbers of joints are present.

Joint sets identified from the pavements are based on a total of 137 joint orientations, combined from all four pavements, while joint groups in this study are based on a total of 50 joint orientations. The northeast-trending joint group identified at field stations has a narrower range in azimuth than the northeast-trending set identified from the pavements, possibly due to the lower sample size obtained in this study. Although the total number of cooling joints identified in this study is low, a bimodal distribution is apparent.

Trace Lengths

Fracture trace abundance (the number of fracture traces per unit area) and fracture-trace length data collected from cleared pavements in the upper lithophysal unit (Barton and Larsen, 1985; Christopher C. Barton and others, USGS, written commun., 1985) were used to evaluate trace abundance (the number of traces per unit area) from aerial-photo data in this unit. Similar data collected for this study at field stations (uncleared outcrops) were used to evaluate photo data from stations in the undifferentiated lower lithophysal and hackly and caprock units. For reasons discussed in a previous section, the photogeologic study eliminates traces having actual lengths less than 3.2 m. The pavement studies show that 66-87 percent of the fracture traces exposed on the four pavements are 3.2 m or less in length. If this is true generally, a maximum of about 34 percent of all fracture traces that exist would be recorded on the photogeologic map even under optimum circumstances of 100 percent exposure. The remainder of the fracture traces would not be detectable or measurable on the aerial photographs. Because rock exposure is not complete, only a small percentage of the actual fracture population is detectable on the aerial photographs. These two factors eliminate more than 66-87 percent of the fracture population.

Table 1 lists, for each station, both the number of field-measured fractures that have traces longer than 3 m and the total number of photogeologic traces (each of which, as discussed previously, is greater than 3.2 m in length). Using trace-length data, the number of photogeologic traces mapped is greater than the number of field-observed fractures at all stations, suggesting that many of the photogeologic traces are erroneous. Two possible explanations for this discrepancy are offered. (1) While two or more short, similarly striking fractures, positioned nearly end to end, were distinquishable in the field, they may have appeared as one linear feature (greater than 3.2 m long) on the aerial photos. Similarly, two crossing fractures with different strikes or two fractures in which one fracture abuts

Table 1.--Trace-length distributions at photo stations and field stations

Station number	Aerial photo stations (No. of traces >3.2 m long)	Field stations (No. of fracture traces >3 m long)
Undifferentiated lower lithophysal and hackly unit		
50	11	6
Upper lithophysal unit		
42	13	2
45	14	2
47	16	0
Caprock unit		
24	36	5
43	13	12
44	11	6
46	15	6
52	35	0

the other fracture may have appeared as a single curved feature on the aerial photos. (2) Some of the linear features plotted on the photogeologic map were determined in the field to be fractures caused by surficial weathering and were not recorded. Field observation confirms that fractured edges of displaced blocks of bedrock were plotted from the aerial photographs on Yucca Crest. Ledges, created by exfoliation jointing and eliminated in the field may have been visible as linear features on the aerial photographs. By both these means, fractures that were either eliminated, or observed as less than 3 m long in the field, may have been recorded on the photogeologic map.

Trace Abundances

Table 2 lists for each station, the number of fracture traces recorded in the field and the number of photogeologic traces mapped from the aerial photographs. Table 2 also lists the number of fracture traces mapped from cleared pavements (Christopher C. Barton and others, USGS, written commun., 1985). Numbers of fracture traces measured at each field station range from 0 to 100, in areas ranging in size from 153 to 1244 m^2. In the upper lithophysal unit, data from pavement studies (Barton and Larsen, 1985; Christopher C. Barton and others, USGS, written commun., 1985) and field data collected in this study can be used to evaluate photogeologic trace abundances. Fracture-trace abundances from pavements 100, 200, 300, and 600, are 1.03, 0.39, 1.12, and 1.28 fractures per square meter, or an average of 0.94 fractures per square meter. Because Barton and Larsen (1985) have shown that fracture abundance changes laterally within this unit, the average fracture abundance is used only as a general guide for evaluating fracture abundances in the upper lithophysal unit, rather than as a precise standard or a reliable predictor.

Fracture-trace abundances at field stations in the upper lithophysal unit range from 0.10 to 0.17 fractures per square meter (table 2). Compared to the average fracture abundance of 0.94 fractures per square meter documented from the pavements, only about 11-18 percent of the total fractures are observed at field stations. Trace abundances from corresponding aerial-photo stations range from 0.02 to 0.03 fractures per square meter, or only about 2 to 3 percent of the average pavement fracture abundance. These numbers are probably too low to characterize the fracture patterns.

Because no pavements have been mapped in the undifferentiated lower lithophysal and hackly and caprock units, actual fracture abundances for these units are not known. Field data collected during this study from these two units provide the only means of comparing trace abundances at the aerial-photo stations. Field station 50, located within the undifferentiated lower lithophysal unit, has a fracture-trace abundance of 0.65 fractures per square meter (based on 100 fractures measured), the highest fracture frequency found at any field station. At the same station, only 0.07 traces per square meter were recorded from aerial photographs, corresponding to about 11 percent of the fracture traces recorded at field station 50. Furthermore, only 6 of 100 fracture traces measured at field station 50 were longer than 3 m while all 11 traces recorded on the aerial photographs at station 50 were longer than 3.2 m. Therefore, at least some of the photogeologic traces mapped at station 50 are erroneous.

Table 2.--Trace abundances from stations in this study and from pavement studies

[Leaders, --, indicate not determined]

Station Number	Area (m^2)	Number of traces[1] Total	Cooling	Unspecified	Total traces[1] per square meter
Undifferentiated lower lithophysal and hackly unit					
50	153	11 (100)	--(--)	11 (100)	0.07 (0.65)
Upper lithophysal unit					
42	697	13 (73)	--(15)	13 (58)	0.02 (0.10)
45	576	14 (100)	--(25)	14 (75)	0.02 (0.17)
47	465	16 (80)	--(10)	16 (70)	0.03 (0.17)
Pavements[2]					
100	214	(221)	(70)	(151)	(1.03)
200	260	(102)	(9)	(93)	(0.39)
300	221	(248)	(49)	(199)	(1.12)
600	250	(321)	(9)	(312)	(1.28)
Caprock unit					
24	840	36 (05)	--(--)	36 (05)	0.04 (0.01)
43	372	13 (23)	--(--)	13 (23)	0.03 (0.06)
44	413	11 (22)	--(--)	11 (22)	0.03 (0.05)
46	479	15 (41)	--(--)	15 (41)	0.03 (0.09)
52	1244	35 (0)	--(--)	35 (0)	0.03 (0.00)

[1]Numbers not set off by parentheses refer to data from aerial photographs; numbers in parentheses refer to data gathered in the field.
[2]Data from Christopher C. Barton and others (USGS, written commun., 1985).

Fracture-trace abundances and photogeologic-trace abundances are very low for field and photo stations located in the caprock unit. The author considers these numbers too low to compare. Numbers of traces recorded from photo stations 24 and 52, are 36 and 35, respectively. The stations are located within the caprock unit on Yucca Crest. Most of the linear features plotted from the photographs on Yucca Crest were visible as faint lines. Only five fractures were observed at field station 24; no fractures were observed at field station 52. Therefore, nearly all of the traces obtained from the aerial photos at these stations are erroneous. Field observations revealed two probable causes. (1) Bedrock at Yucca Crest is concealed by extensive talus and a thin soil cover. Only a few isolated, displaced blocks of bedrock were exposed. On the aerial photographs, these blocks appeared to be in place, and their edges were seen and mapped as linear features. (2) In addition, fractures, determined to be the result of surficial weathering and eliminated as part of the field data, may have appeared as linear features on the aerial photographs. The author believes that both these factors played a role in the mapping of erroneous traces at photo stations 24 and 52.

The large number of linear features, seen as faint lines on the photographs on Yucca Crest were not discernible in the field. It is possible that they may represent fracture traces covered by a thin soil veneer, and thus, were not discernible in the field. Based on field observations, the few fracture traces visible on the photographs on Yucca Crest are fractured edges of displaced rock, caused by surficial weathering. Because almost all of the linear features (mostly faint lines) mapped on Yucca Crest from photographs cannot be definitively related to fracture traces, the data from Yucca Crest must be considered erroneous.

Summary Of Data Analysis

Cooling joint orientations identified at field stations are distinguished by two well-defined groups ranging from 15° to 47° and 300° to 350°, but their orientations show little resemblance to bearings of photogeologic traces measured from the photogeologic map. Field station 46 shows a well-defined grouping of fractures other than cooling joints, ranging from 325° to 359°, but similar orientations from the corresponding photo station are absent. At other field stations, fractures, other than cooling joints, cannot be separated into well-defined groups. Because joint groups identified at field stations are similar to joint sets identified at pavements, it may be possible to characterize the joint population from incompletely exposed outcrops, even when low numbers of joints are present.

Trace bearings measured from the aerial photos do not agree with fracture-trace bearings measured in the field. Groups present in the field are missing or are poorly represented in photo counterparts. For all stations, the number of photogeologic traces mapped (all greater than 3.2 m long) exceeds the number of fracture traces greater than 3 m long observed at corresponding field stations; thus, many of the photogeologic traces are erroneous. Because the orientations do not agree, and because trace-length data show numerous photogeologic traces to be erroneous, the photogeologic map includes linear features at first thought to be fracture traces, but which cannot be related to fracture traces.

The low numbers of linear features recorded on the photogeologic map compared to those recorded at field stations confirm that the numbers of photogeologic traces recorded are insufficient to adequately characterize the actual fracture patterns on the ground. The extremely low ratio of traces recorded on the photogeologic map at stations located in the upper lithophysal unit, compared to the average fracture abundance in the pavements, emphasizes that the photogeologic mapping eliminated far too many traces for the photogeologic map to reliably and consistently characterize the actual fracture pattern in this unit. This conclusion holds true for the other units studied as well.

LIMITATIONS OF STUDY

Many of the problems encountered in this study are inherent in most photogeologic studies of linear features. Even with good-quality photographs and a high-precision stereoplotting instrument such as the Kern PG 2 plotter, factors such as photographic scale, tonal contrast, film type, filter, and resolution of the photographic details influence the interpretation of aerial photographs. A detailed discussion of these factors is beyond the scope of this report, and the reader is referred to Ray (1960) for additional information.

The photogeologic map produced in this study does not reflect the actual distribution of linear features in the units studied, because photographic scale, photo quality and resolution, degree of exposure, and topographic relief, in addition to the actual distribution of traces, determined what is visible on the air photos. In this study, bedrock was concealed in many areas by soil, talus, and vegetation, severely limiting visibility.

One factor inherent in most photogeologic studies, and which greatly influenced this study, is vertical exaggeration. This phenomenon so reduced the visibility of linear features on slopes, that primarily only ridgetops were mapped. This greatly restricted the scope of the study because only three of seven units of the Tiva Canyon Member are exposed on the ridgetops.

A problem unique to this study was dictated by the method chosen to verify the linear features mapped from the air photos. Areas were chosen on the photogeologic map where linear features were abundant and located solely within one unit. These areas are often poorly exposed in the field, and conversely, areas of good exposure in the field often show few traces on the photographs. This resulted in difficulty comparing photogeologic traces with field-measured fracture traces.

It was not possible to distinguish between joints, or faults with small displacements on the photographs. Although fractures are two-dimensional, only one dimension is generally represented on aerial photographs; two dimensions are seen only when a portion of the fracture face is visible. Because the topographic surface was not generally horizontal, only the surface expression (trace) of the linear features was seen on the air photos, not actual strikes. In addition, because only a portion of any linear trace is visible on the aerial photos, only minimum trace lengths were obtained.

CONCLUSIONS

Most of the difficulties encountered in this study evolved from limitations or problems resulting from the photographic scale coupled with poor exposures. The 1:2400 photographic scale, although unusually large for a study of this type, nevertheless was not adequate to discern the majority of fracture traces exposed on the ground. In addition, soil and extensive talus conceal bedrock and limit visibility. As a result, Yucca Mountain, and particularly Yucca Crest, is poorly suited to this type of aerial photo study. Many linear features that resemble fracture traces on the aerial photos proved not to be fractures in the field, so that part--perhaps a substantial part--of the photogeologic map is erroneous. Thus, the linear features mapped from aerial photographs do not realistically characterize the fracture networks actually present.

ACKNOWLEDGMENTS

Richard W. Spengler proposed the study. The author wishes to thank Richard W. Spengler, Christopher C. Barton, Earl R. Verbeek, and Robert B. Scott, all of the U.S. Geological Survey, Denver, Colorado, for their guidance and valuable suggestions. Eric Larsen and Patrica E. Baechle of Fenix & Scisson, Inc., Las Vegas, Nevada, assisted in field work.

REFERENCES

Barton, C.C., Howard, T.M., and Larsen, Eric, 1984, Tubular structures on the faces of cooling joints: a new volcanic feature: Transactions of the American Geophysical Union, EOS, v. 65, no. 45, p. 1148.

Barton, C.C., and Larsen, Eric, 1985, Fractal geometry of two-dimensional fracture networks at Yucca Mountain, southwestern Nevada: Proceedings of the International Symposium on Fundamentals of Rock Joints, Bjorkliden, Lapland, Sweden, September 15-20, 1985, p. 77-84.

Barton, Nick, and Choubey, Vishnu, 1977, The shear strength of rock joints in theory and practice: Rock Mechanics, v. 10, p. 1-54.

Beatley, J.C., 1976, Vascular plants of the Nevada Test Site and central-southern Nevada: Ecologic and Geographic Distributions: U.S. Energy Research and Development Administration Report TID-26881, 308 p.

Brown, D.E., Lowe, C.H., and Pase, C.P., 1979, A digitized classified system for the biotic communities of North America, with community (series) and association examples for the Southwest: Journal of the Arizona Academy of Science, v. 14, supplement 1, 16 p.

Carr, W.J., 1974, Summary of tectonic and structural evidence for stress orientation at the Nevada Test Site: U.S. Geological Survey Open-File Report 74-176, 53 p.

Houghton, J.G., Sakamoto, C.M., and Gifford, R.O., 1975, Nevada's weather and climate: Nevada Bureau of Mines Special Publication 2, 78 p.

Ray, R.G., 1960, Aerial photographs in geologic interpretation and mapping: U.S. Geological Survey Professional Paper 373, 230 p.

Scott, R.B., Bath, G.D., Flanigan, V.J., Hoover, D.B., Rosenbaum, J.G., and Spengler, R.W., 1984, Geological and geophysical evidence of structures in northwest-trending washes, Yucca Mountain, southern Nevada, and their possible significance to a nuclear waste repository in the unsaturated zone: U.S. Geological Survey Open-File Report 84-567, 23 p.

Scott, R.B., and Bonk, Jerry, 1984, Preliminary geologic map of Yucca Mountain, Nye County, Nevada with geologic sections: U.S. Geological Survey Open-File Report 84-494, scale 1:12,000.

Snyder, C.T., Hardman, George, and Zdenek, F.F., 1964, Pleistocene lakes in the Great Basin: U.S. Geological Survey Miscellaneous Geological Investigations Map I-416, scale 1:100,000.

Snyder, D.B., and Carr, W.J., 1982, Preliminary results of gravity investigations at Yucca Mountain and vicinity, southern Nye County, Nevada: U.S. Geological Survey Open-File Report 82-701, 36 p.

Spaulding, W.G., 1985, Vegetation and climates of the last 45,000 years in the vicinity of the Nevada Test Site, south-central Nevada: U.S. Geological Survey Professional Paper 1329, 83p.

Stewart, J.H., and Carlson, J.E., 1978, Geologic map of Nevada: U.S. Geological Survey, scale 1:500,000.

U.S. Geological Survey, 1984, A summary of geologic studies through January 1, 1983, of a potential high-level radioactive waste repository site at Yucca Mountain, southern Nye County, Nevada: U.S. Geological Survey Open-File Report 84-792, 103 p.

Wu, S.S.C., compiler, 1985, Topographic maps of Yucca Mountain area, Nye County, Nevada: U.S. Geological Survey Open-File Report 85-620, scale 1:5000, 6 sheets.

APPENDICES I-III

Data in Appendices I-III are organized by the geologic units in which they occur. Directions of photogeologic traces and field-measured fracture traces were originally recorded in bearings and later converted to azimuth to facilitate entry into a computer data base. Azimuths of linear features measured from the photogeologic map are listed in Appendix I. Appendix II contains fracture data obtained at field stations. The first column in Appendix I contains the linear feature number; the second column gives the azimuth. In Appendix II, the first column contains the fracture number. Numbers assigned the prefix symbol "J" designate fractures identified as cooling joints. The third column of Appendix II records dip angle and dip quadrant; the fourth column is the length category, and the fifth column contains supplementary field observations. The symbol cl, found in the fifth column, designates fractures which cut lithophysae. This observation was recorded because cooling joints at Yucca Mountain have not been observed to cut lithophysae. The symbol ws in the fifth column designates fractures with weathered surfaces. Fracture traces which were observed to curve in the field are noted in the fifth column. Appendix III contains histograms of trace orientation data obtained in the field and from the aerial photographs. Also included in Appendix III is a combined orientation data plot of cooling joints identified in this study and those identified from pavements 100, 200, 300, and 600.

APPENDIX I

Azimuths of linear features measured from the photogeologic map

Undifferentiated lower lithophysal and hackly unit of the Tiva Canyon Member

PHOTO STN 50

Linear Feature Number	Azimuth
44	287
45	310
46	342
47	342
48	346
49	346
50	348
51	15
52	18
53	40
54	42

Upper lithophysal unit of the Tiva Canyon Member

PHOTO STN 42		PHOTO STN 45		PHOTO STN 47	
Linear Feature Number	Azimuth	Linear Feature Number	Azimuth	Linear Feature Number	Azimuth
1	50	14	312	28	284
2	303	15	321	29	293
3	303	16	328	30	305
4	315	17	335	31	323
5	321	18	341	32	326
6	333	19	350	33	329
7	39	20	358	34	342
8	39	21	36	35	347
9	59	22	51	36	349
10	55	23	52	37	13
11	64	24	73	38	19
12	86	25	79	39	23
13	87	26	79	40	41
		27	79	41	57
				42	66
				43	66

Caprock unit of the Tiva Canyon Member

PHOTO STN 24		PHOTO STN 43		PHOTO STN 44	
Linear Feature Number	Azimuth	Linear Feature Number	Azimuth	Linear Feature Number	Azimuth
55	295	91	314	104	283
56	295	92	337	105	305
57	345	93	337	106	348
58	345	94	337	107	348
59	337	95	344	108	2
60	340	96	342	109	18
61	31	97	15	110	15
62	31	98	20	111	59
63	44	99	63	112	79
64	46	100	73	113	85
65	46	101	77	114	90
66	8	102	20		
67	349	103	356		
68	303				
69	28				
70	13				
71	344				
72	336				
73	337				
74	3				
75	39				
76	39				
77	348				
78	54				
79	348				
80	55				
81	304				
82	59				
83	345				
84	67				
85	354				
86	330				
87	47				
88	31				
89	330				
90	342				

Caprock unit of the Tiva Canyon Member

PHOTO STN 46

Linear Feature Number	Azimuth
115	89
116	289
117	298
118	309
119	317
120	317
121	340
122	46
123	46
124	289
125	289
126	333
127	322
128	326
129	332

PHOTO STN 52

Linear Feature Number	Azimuth
130	40
131	39
132	316
133	36
134	1
135	39
136	39
137	340
138	25
139	25
140	41
141	358
142	358
143	349
144	313
145	44
146	48
147	48
148	309
149	74
150	74
151	327
152	321
153	74
154	35
155	80
156	26
157	3
158	3
159	39
160	39
161	300
162	309
163	319
164	309

APPENDIX II

Fracture-trace orientations (azimuth and dip), length category, and observations from data collected in the field

Symbols used in Appendix II

J = fractures identified as cooling joints

cl = fracture surface cuts lithophysae

ws = fracture surface is weathered

Undifferentiated lower lithophysal and hackly unit of the Tiva Canyon Member

FIELD STN 50

Fracture Number	Azimuth	Dip	Length Category	Observations
254	359	84E	2	cl, ws
255	303	85E	2	cl
256	85	90	2	cl
257	336	85E	3	cl, ws
258	58	30W	2	cl
259	352	84E	2	cl
260	352	84E	2	cl, curves, abuts #259
261	351	87E	2	cl
262	347	72E	3	cl
263	357	82W	3	cl, curves, abuts #265
264	356	76W	3	cl, curves
265	303	67E	3	cl, curves
266	30	84W	3	cl
267	280	79W	3	cl
268	319	75W	3	cl
269	341	89W	2	cl
270	352	82E	3	cl
271	0	73W	1	cl, curves
272	307	82W	3	cl
273	307	85W	2	cl
274	308	80W	1	cl
275	350	90	3	cl
276	75	84W	3	
277	44	90	3	ws
278	324	58E	3	cl, ws
279	28	79W	3	cl
280	311	88E	3	cl
281	306	85E	2	cl
282	323	75E	3	
283	336	76W	3	
284	39	75W	3	cl
285	331	90	3	
286	284	76W	2	cl
287	317	52W	2	cl, curves
288	320	90	2	cl, ws, curves
289	305	90	2	cl
290	288	86W	3	
291	316	76W	3	
292	355	70W	3	cl, curves
293	307	74W	3	cl
294	349	66W	2	cl
295	345	83W	3	cl

FIELD STN 50--Continued

Fracture Number	Azimuth	Dip	Length Category	Observations
296	305	82W	3	
297	32	87E	3	cl
298	5	86E	1	cl, curves
299	80	69W	2	cl, curves
300	354	63W	3	cl, curves
301	357	90	3	cl
302	323	82W	3	cl, curves
303	304	79W	1	cl
304	347	70W	2	cl
305	347	74W	3	cl
306	48	74W	1	cl
307	74	84E	2	cl, ws, curves
308	22	90	1	cl, ws
309	26	67W	2	cl, ws
310	352	81E	3	cl
311	324	63W	3	cl, #311, #312 are part of swarm of at least 5
312	327	82W	3	cl, see #311
313	324	53W	2	cl
314	330	75W	3	cl
315	54	87E	2	cl
316	350	74W	3	cl
317	353	73W	3	
318	351	84W	3	
319	346	70W	3	cl
320	346	66W	3	cl
321	343	78W	3	cl
322	355	82W	3	cl
323	295	84W	3	cl
324	333	53W	3	cl
325	32	90	3	
326	351	70W	3	
327	300	78W	3	
328	280	71W	3	cl
329	315	75W	3	
330	307	84W	2	cl
331	340	63W	3	abuts #330
332	304	81W	3	
333	346	65W	3	cl
334	303	80W	3	
335	298	87W	3	cl
336	297	66W	3	cl
337	343	82W	2	cl
338	8	82W	3	cl
339	8	82W	3	cl
340	272	79W	3	cl, ws

FIELD STN 50--Continued

Fracture Number	Azimuth	Dip	Length Category	Observations
341	272	75W	3	cl, sinuous trace
342	356	80E	3	cl
343	343	83W	3	cl
344	309	88W	3	cl
345	355	79W	3	
346	305	80W	3	
347	320	72W	3	#347, #348 are part of swarm of at least 4
348	319	74W	3	cl, see #347
349	340	90	2	cl
350	295	90	3	cl
351	70	73E	3	cl, curves
352	72	90	3	cl
353	297	70W	3	cl

Upper lithophysal unit of the Tiva Canyon Member

FIELD STN 42

Fracture Number	Azimuth	Dip	Length Category	Observations
J1	20	82W	3	ws
2	327	77W	2	cl
3	328	86W	3	cl
4	328	86W	3	cl
5	12	74W	3	cl
6	340	88W	3	cl
7	325	86W	3	cl
8	345	83W	3	cl
9	340	86W	3	cl
J10	300	82W	3	ws
11	320	82W	3	curves
J12	26	87W	3	
13	30	90	3	cl
14	325	85E	3	cl, curves, #14, #17, #18 are part of a swarm
15	5	75W	2	cl
16	320	83W	3	cl
17	315	82E	3	cl, curves, see #14
18	328	90	2	cl, curves, see #14
19	42	86W	3	cl
20	7	80W	3	cl, ws
21	335	79W	3	cl, curves
22	330	66W	3	cl, curves
J23	35	76W	2	
J24	40	69W	2	
25	320	82W	3	cl
26	3	90	3	cl
27	40	78E	3	cl
28	352	88W	2	cl, curves
29	337	90	3	cl, curves
30	319	74W	3	cl
J31	34	83W	2	
J32	20	83W	3	
J33	304	81E	2	
J34	20	84W	3	
35	342	88W	2	cl, curves
36	40	74E	3	cl
J37	28	74W	2	
J38	29	72W	2	
39	345	81W	3	cl, #39, #40, #41, are part of swarm
40	345	84W	3	cl, curves, see #39
41	344	79W	3	cl, see #39
42	340	87W	3	cl
43	355	80W	1	cl, ws, curves

FIELD STN 42--Continued

Fracture Number	Azimuth	Dip	Length Category	Observations
J44	27	76W	2	
J45	28	82W	2	
J46	28	76W	2	
47	32	77E	3	cl
48	355	85W	3	cl
49	320	85W	2	cl
50	335	78W	1	cl
51	338	74W	3	cl, curves
52	323	84E	3	cl
53	294	84W	3	cl
54	4	86W	3	cl, curves
55	355	80W	3	cl, sinuous trace
56	300	88W	3	cl
57	292	90	3	cl
58	355	85W	3	cl
59	325	73W	3	cl
60	40	82W	3	cl
61	322	84W	3	cl
62	35	86E	3	cl
63	337	62W	3	cl
64	326	80W	3	cl, #64, #65 are part of swarm of 6 or more
65	325	72W	3	cl, see #64
66	320	90	3	cl
67	320	72E	3	cl
68	18	84E	3	cl
69	325	79W	2	cl
70	312	83W	2	cl, curves
J71	28	76W	3	
72	275	83W	3	cl, curves
73	75	89W	3	cl

FIELD STN 45

Fracture or Joint Number	Azimuth	Dip	Length Category	Observations
J74	350	83E	2	
75	75	80E	3	
76	55	90	3	
77	330	67W	3	
78	340	72W	3	
79	335	65W	3	
J80	310	89W	3	
81	349	72W	2	
82	59	90	3	

FIELD STN 45--Continued

Fracture Number	Azimuth	Dip	Length Category	Observations
J83	346	82E	3	
84	309	81W	3	cl
J85	40	77W	2	
J86	34	64W	3	curves
87	320	90	3	
J88	335	85W	3	
J89	319	86W	3	
90	325	54W	3	cl
91	332	62W	3	cl
92	323	82W	3	
J93	45	77W	3	
J94	320	83E	2	
95	9	71W	3	
J96	26	85W	3	
97	0	80W	3	
98	357	86W	3	
J99	315	77E	3	
100	5	82E	3	cl
J101	35	81W	1	
102	350	60E	3	
103	344	74W	3	
104	45	89E	3	
105	83	88E	3	curves
106	350	82E	3	cl
107	22	56W	3	
108	40	82W	3	cl
109	350	71E	3	
110	340	53W	3	ws
111	300	90	3	
112	349	66W	3	
113	90	63S	3	
114	29	79W	3	cl
115	03	85W	3	cl
116	310	73E	3	cl
117	323	83W	3	cl
J118	38	82E	3	
119	331	71E	3	cl
120	331	76W	2	cl
121	354	73E	2	cl, sinuous trace
122	40	84E	3	cl
123	340	79E	3	
124	345	90	3	cl
125	345	80E	3	cl
126	340	70E	2	cl, sinuous trace
127	280	84W	3	cl
128	290	57W	3	cl
129	335	70E	3	cl
130	323	90	3	cl

FIELD STN 45--Continued

Fracture Number	Azimuth	Dip	Length Category	Observations
131	290	83W	3	cl
132	287	90	3	cl
133	340	80E	3	cl, curves
134	312	65E	3	
135	336	84E	3	cl
136	350	70E	3	cl
137	343	84W	3	cl
138	323	90	3	cl
139	345	70W	3	cl
140	347	72W	3	cl
141	348	60E	3	cl
J142	18	79E	3	
143	337	75E	3	cl
144	340	77W	3	cl
145	336	84W	3	cl
J146	42	86E	3	
J147	20	89E	1	curves
J148	318	85W	3	
J149	25	83W	3	
150	323	85W	2	cl
151	47	62W	3	cl
J152	37	78E	3	
153	348	90	3	cl
J154	40	79E	3	
J155	310	90	3	ws
J156	343	74E	3	curves
J157	320	84W	3	ws
158	36	62E	3	cl
159	348	85E	3	cl
160	0	82W	3	cl
161	347	90	3	cl
162	348	86W	3	cl
163	331	80W	3	cl
164	350	76W	3	cl
165	348	67W	3	cl
166	275	72E	3	cl
167	338	83E	3	cl
J168	40	87E	3	ws
169	325	65E	3	cl, ws
170	310	80W	3	cl
J171	42	90	3	ws
172	324	74W	3	cl
173	5	71W	3	cl

STATION 47

Fracture Number	Azimuth	Dip	Length Category	Observations
J174	334	85E	2	ws
175	337	68W	3	cl
176	340	86W	3	cl
177	347	84E	3	cl, curves, #177-181 comprise a swarm
178	4	90	3	cl, curves, see #178 of swarm
179	11	81E	3	cl, curves, see #178
180	11	81E	3	cl, curves, see #178
181	15	76E	2	cl, curves, see #178
182	351	85W	3	cl
J183	348	82W	3	
J184	337	80E	2	
J185	337	86W	3	
186	2	90	3	cl, #186, #187 are part of swarm of at least 5
187	4	73W	3	cl, see #186
188	346	85E	2	cl
J189	47	70W	3	
190	12	90	3	cl, curves, #190-192 are part of swarm of at least 10
191	10	60W	3	cl, curves, see #190
192	10	58W	3	cl, curves, see #190
J193	278	73W	3	curves
J194	334	81E	3	
195	347	82E	3	cl, curves, #195, #196 are part of swarm of at least 5
196	356	86E	3	cl, curves, see #195
197	307	74W	3	cl
198	339	90	3	cl
199	337	90	3	cl
200	2	71W	3	cl
201	10	76W	3	cl
202	63	56W	2	cl
203	12	90	3	cl
204	47	78W	3	cl
205	15	87W	3	cl
J206	27	79E	3	
207	335	82W	3	cl
208	3	85W	3	cl, curves
209	340	76E	3	cl
210	351	90	3	curves
211	346	82E	3	curves
212	338	81E	3	
213	43	80W	3	
214	350	72E	3	cl
215	345	56E	2	
216	330	90	2	cl, curves

FIELD STN 47--Continued

Fracture Number	Azimuth	Dip	Length Category	Observations
217	350	85E	3	cl
218	25	82E	3	
219	278	74W	3	curves
220	351	70W	3	cl
221	348	80E	3	cl, curves
222	352	85E	3	
223	10	62W	3	cl
224	349	90	3	cl
225	15	85E	3	cl
226	15	85E	3	cl, curves
227	42	77W	3	
228	344	87E	3	
229	355	68W	3	
230	27	65W	3	curves
J231	331	85E	2	
232	8	79W	3	
233	288	65E	3	
234	18	80E	3	
235	335	81W	3	
236	335	75W	3	cl
237	65	77E	3	cl
238	65	90	3	cl
239	75	90	3	cl
J240	15	57W	3	
241	336	79W	3	cl
242	340	67W	3	cl
243	344	74E	2	cl, curves
244	322	81W	3	
245	347	88E	3	
246	90	84S	2	cl, curves
247	345	73E	3	cl
248	64	83E	3	cl
249	64	85E	3	cl
250	346	76E	3	
251	346	86E	3	
252	336	83E	3	cl, curves
253	358	76E	3	cl, curves

Caprock unit of the Tiva Canyon Member

FIELD STN 24

Fracture Number	Azimuth	Dip	Length Category	Observations
440	54	66W	2	ws
441	332	90	3	ws, curves
442	334	90	3	ws, curves
443	330	67E	3	ws
444	352	73E	3	ws

FIELD STN 43

Fracture Number	Azimuth	Dip	Length Category	Observations
354	338	81E	1	cl, ws
355	355	85W	1	ws, curves
356	322	88W	1	ws, curves
357	316	82E	1	ws
358	15	85E	2	ws
359	15	80E	3	ws
360	346	90	3	ws
361	350	82E	3	
362	90	72N	1	ws
363	65	77W	1	ws
364	345	83E	1	ws
365	54	82W	2	ws
366	40	79W	2	ws, curves
367	18	74E	1	ws
368	330	85W	2	ws
369	335	76E	1	ws, curves
370	338	74E	1	ws
371	349	90	1	ws
372	65	83E	1	ws
373	345	75E	3	ws
374	338	83E	3	ws, curves
375	337	70E	3	ws
376	335	83W	3	ws

FIELD STN 44

Fracture Number	Azimuth	Dip	Length Category	Observations
377	62	72W	1	ws
378	300	82E	2	ws, sinuous trace
379	325	75W	2	ws
380	316	88E	2	ws, curves
381	316	84E	2	ws, curves
382	27	87W	3	ws
383	359	64E	1	ws
384	301	78E	3	ws
385	349	32E	3	ws
386	85	77W	2	ws
387	55	76W	1	ws, curves
388	340	76W	1	ws
389	14	74E	1	ws
390	10	90	3	ws
391	345	73E	3	ws
392	3	89E	2	ws
393	48	90	2	cl, ws
394	344	76W	2	ws
395	18	48E	2	ws
396	2	90	3	ws
397	8	82E	3	ws
398	10	86E	1	ws, curves

FIELD STN 46

Fracture Number	Azimuth	Dip	Length Category	Observations
399	347	85E	3	cl, ws
400	349	79E	2	cl, ws, curves
401	340	76W	2	cl, ws, curves
402	335	78W	2	cl, ws, curves
403	339	85W	2	cl, ws, curves
404	345	83W	2	cl, ws, curves
405	55	85W	3	ws, sinuous trace
406	335	74E	3	ws
407	355	84W	3	cl, ws
408	344	68W	2	cl, ws
409	335	72W	2	cl, ws
410	335	71W	2	cl, ws
411	345	70E	3	cl, ws
412	338	65W	1	cl, ws, curves
413	340	88E	1	cl, ws, curves
414	337	79W	2	cl, ws, curves
415	338	70E	3	
416	325	74E	2	cl, curves

FIELD STN 46--Continued

Fracture Number	Azimuth	Dip	Length Category	Observations
417	333	78E	2	cl, ws
418	341	77E	3	cl, ws
419	15	71E	3	cl, ws
420	355	72W	3	cl, ws
421	352	73W	3	cl, ws
422	339	72E	3	cl, ws
423	350	67E	3	cl, ws
424	330	85E	2	cl, ws
425	280	56E	2	cl, ws, curves
426	355	90	1	cl, curves
427	352	88E	2	cl, ws
428	40	56W	3	cl, ws
429	320	90	3	cl, ws
430	348	71W	1	cl, ws, curves
431	40	90	2	cl, ws
432	10	90	2	cl, ws
433	70	77E	1	cl, ws
434	352	68W	1	cl, ws
435	356	90	2	cl, ws
436	22	84W	3	cl, ws
437	325	90	3	cl, ws
438	328	81E	2	cl, ws
439	292	90	3	cl, ws

FIELD STN 52

No fractures were observed in the field

APPENDIX III

Histograms of trace orientation data
obtained in the field and from aerial photographs

Azimuth Frequency Distribution

Air-photo station 50

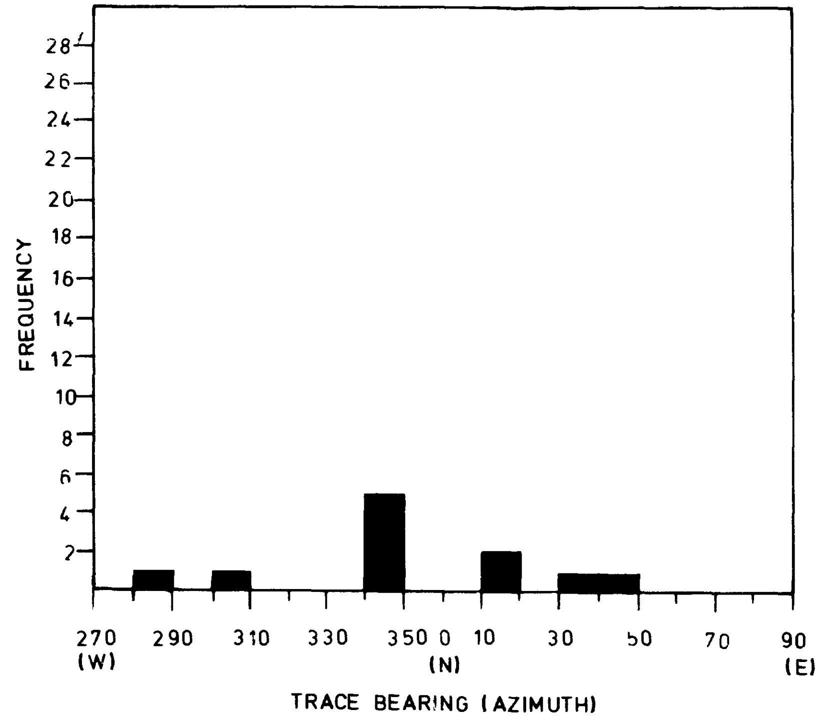

Field station 50

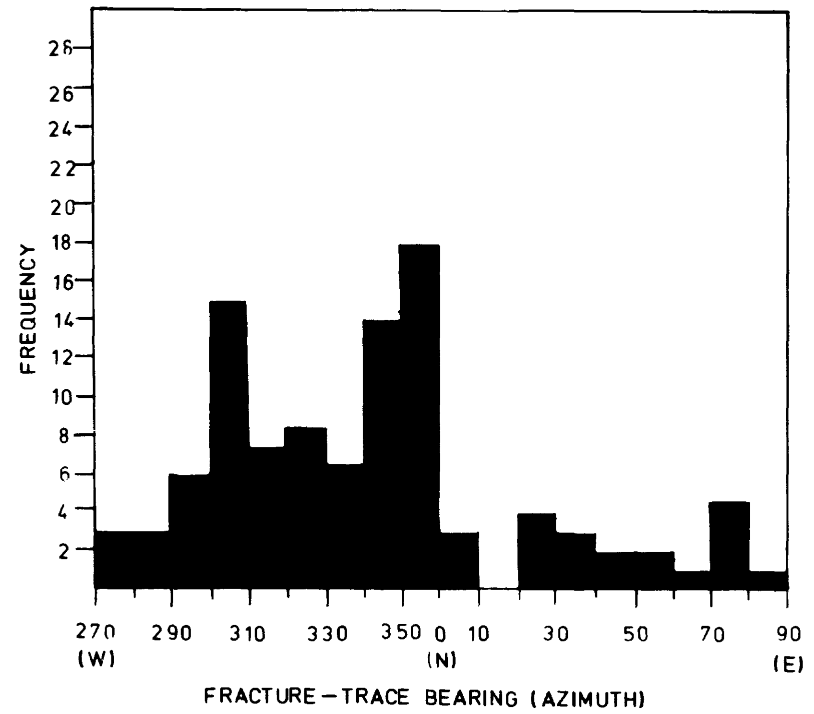

Azimuth Frequency Distribution

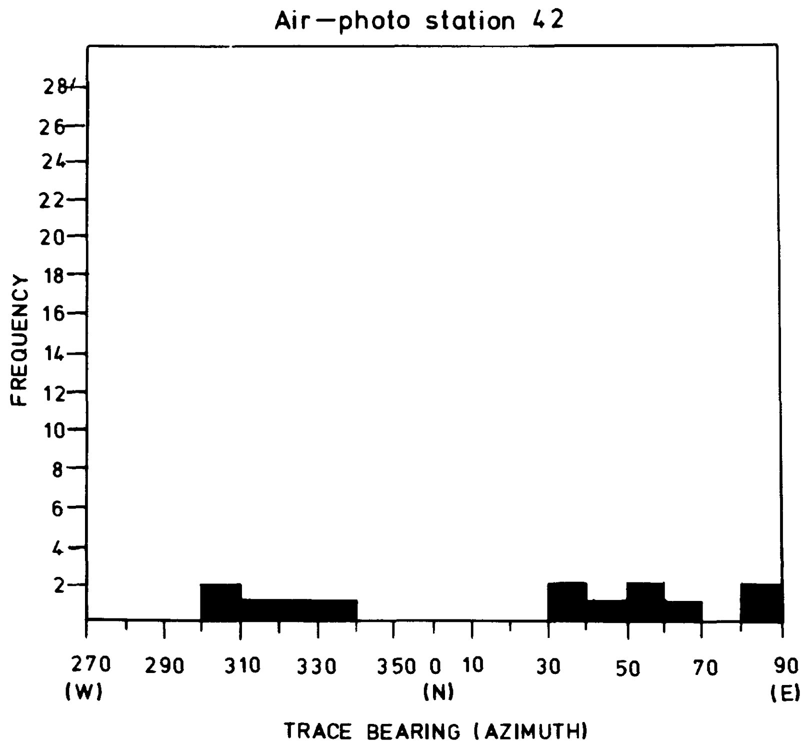

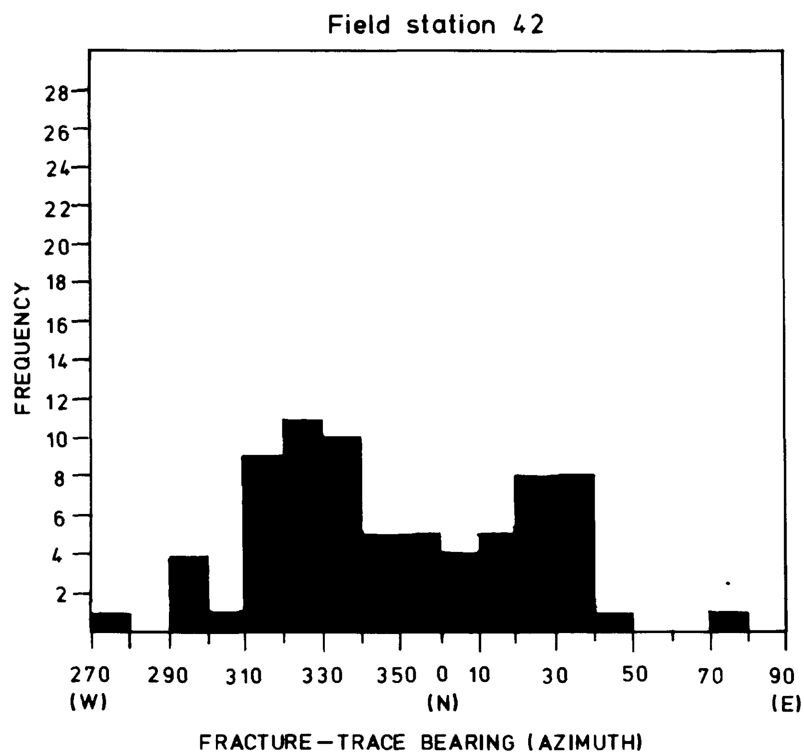

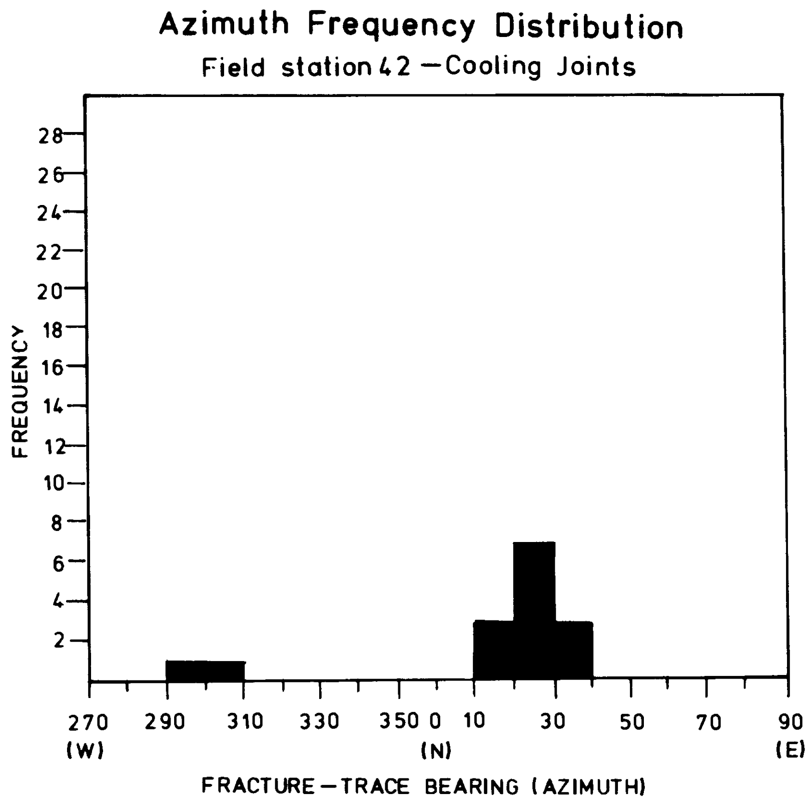
Azimuth Frequency Distribution
Field station 42 —Cooling Joints
FREQUENCY
28
26
24
22
20
18
16
14
12
10
8
6
4
2
270
(W)
290
310
330
350 0
(N)
10
30
50
70
90
(E)
FRACTURE—TRACE BEARING (AZIMUTH)

Combined Azimuth Frequency Distribution

Cooling Joints— Field Stations 42,45,47

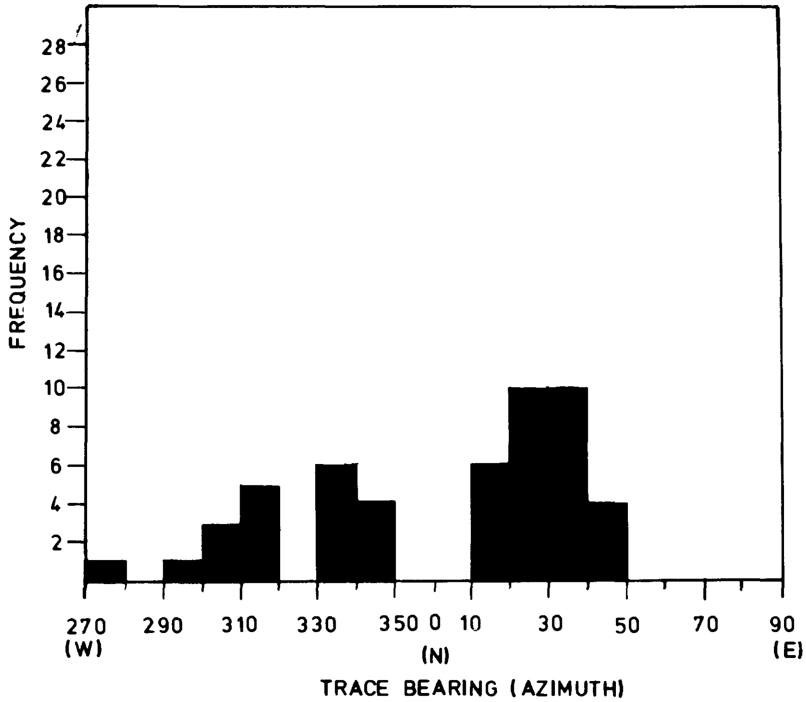

Cooling Joints— Pavements 100,200,300,600

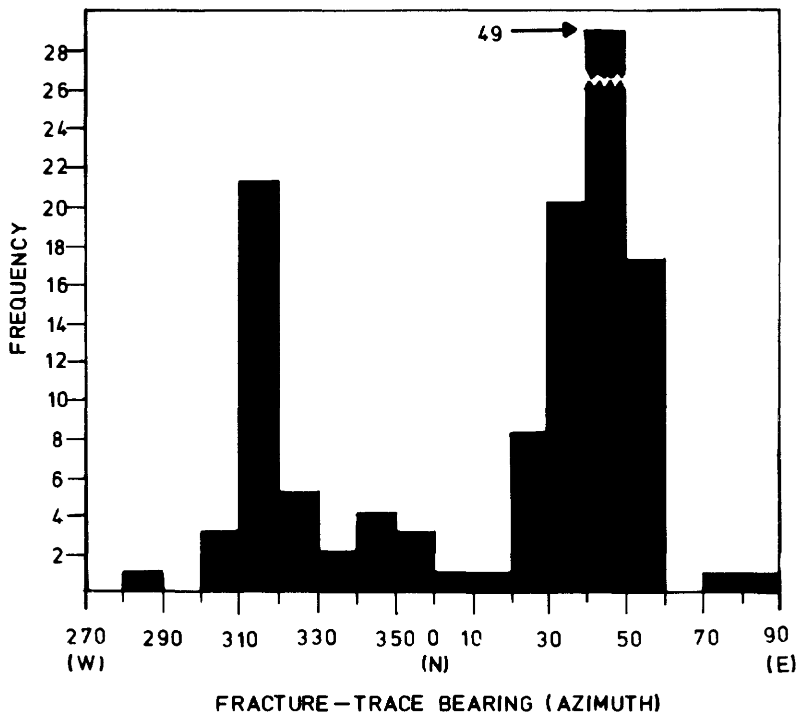

Azimuth Frequency Distribution

Air—photo station 45

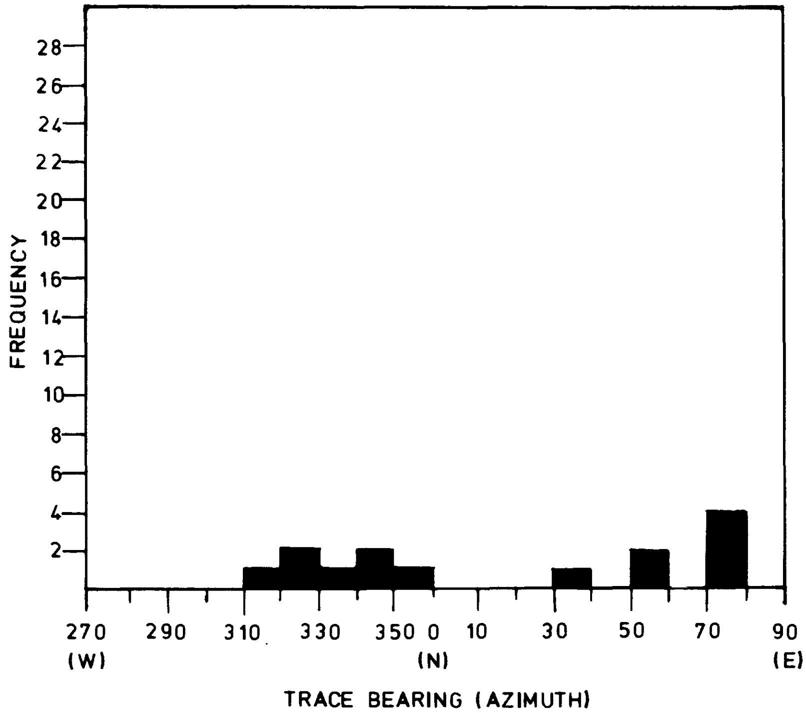

Field station 45

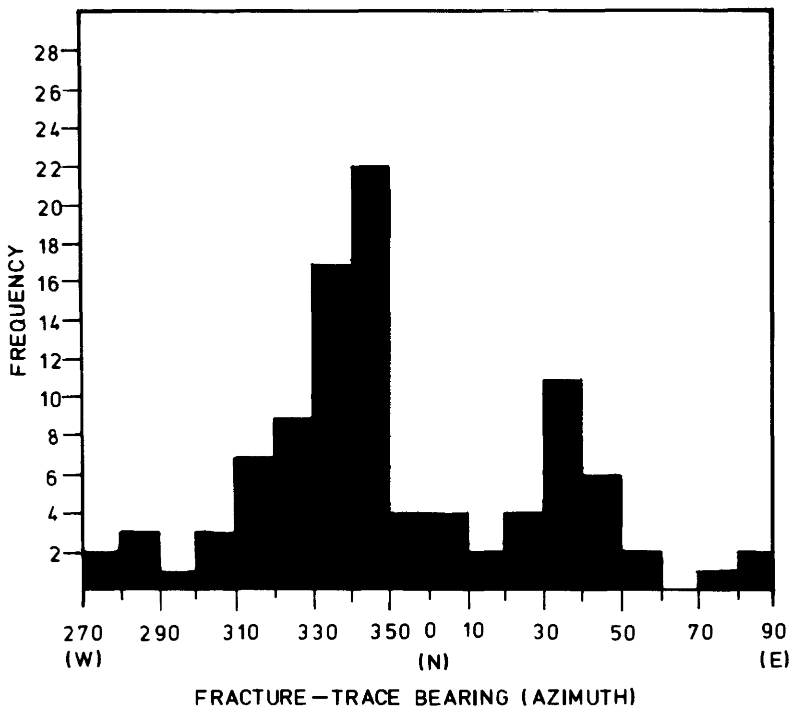

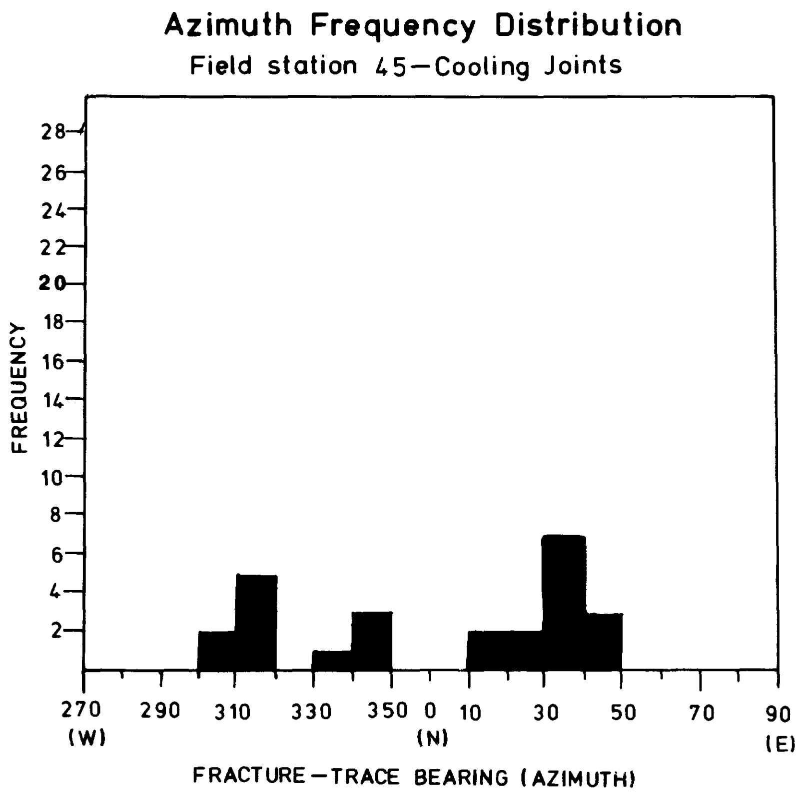
Azimuth Frequency Distribution
Field station 45—Cooling Joints
FREQUENCY
28
26
24
22
20
18
16
14
12
10
8
6
4
2
270 (W)
290
310
330
350
0 (N)
10
30
50
70
90 (E)
FRACTURE—TRACE BEARING (AZIMUTH)

Azimuth Frequency Distribution

Air—photo station 47

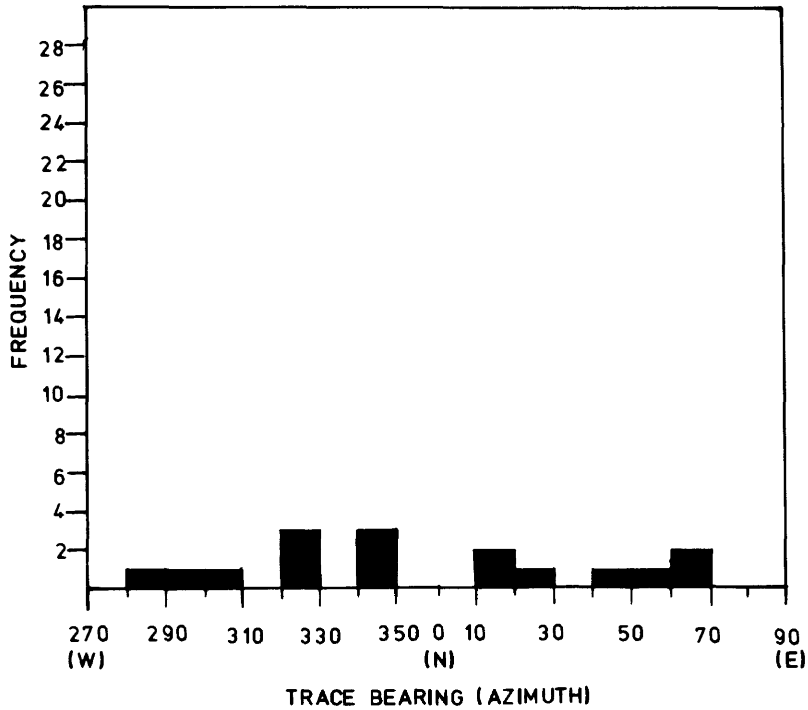

Field station 47

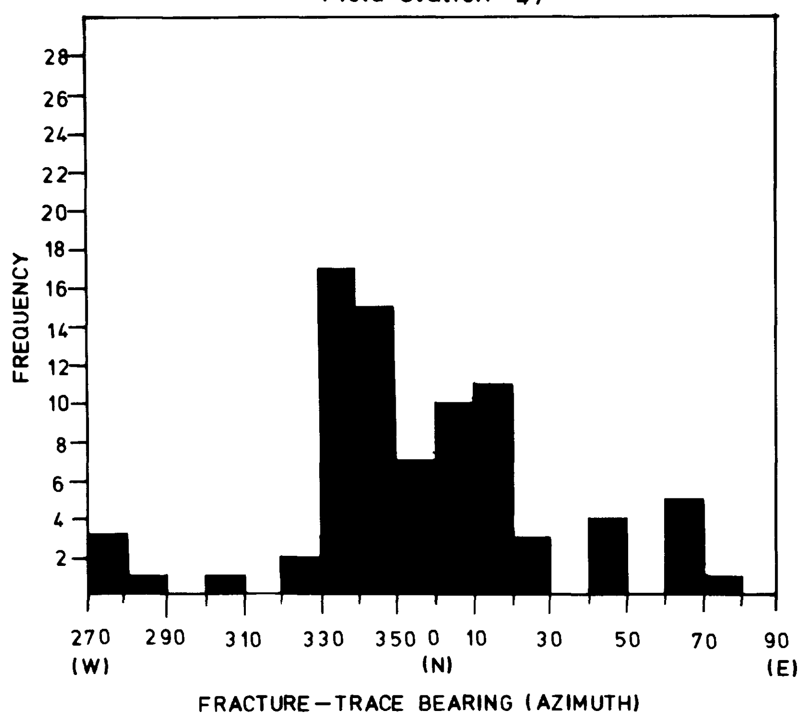

Azimuth Frequency Distribution

Field station 47—Cooling Joints

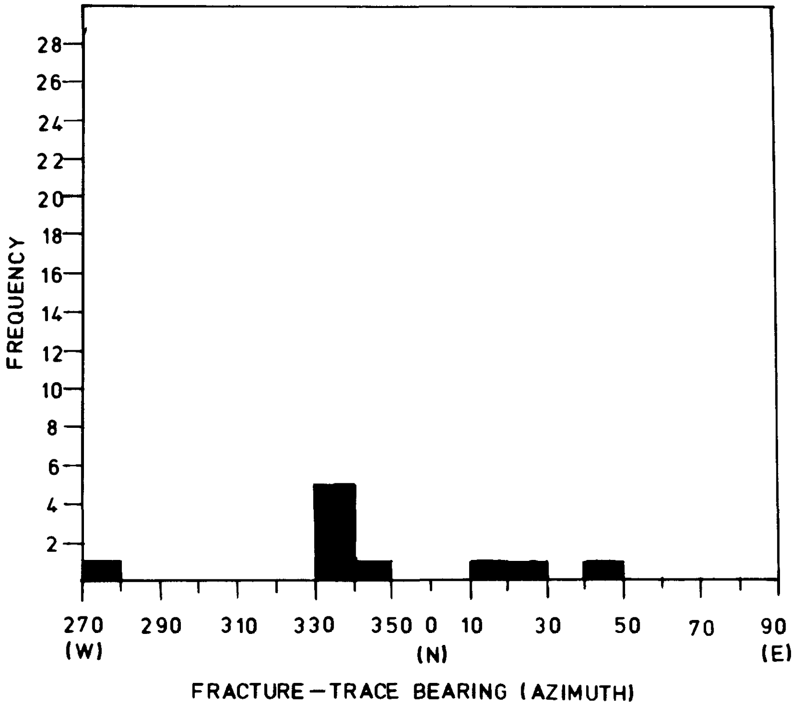

Azimuth Frequency Distribution

Air—photo station 24

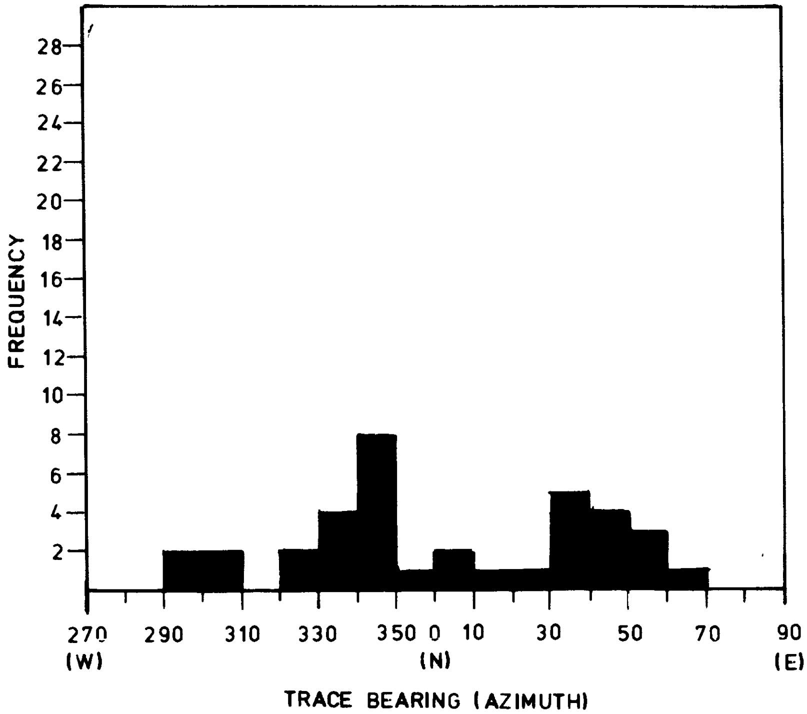

Field station 24

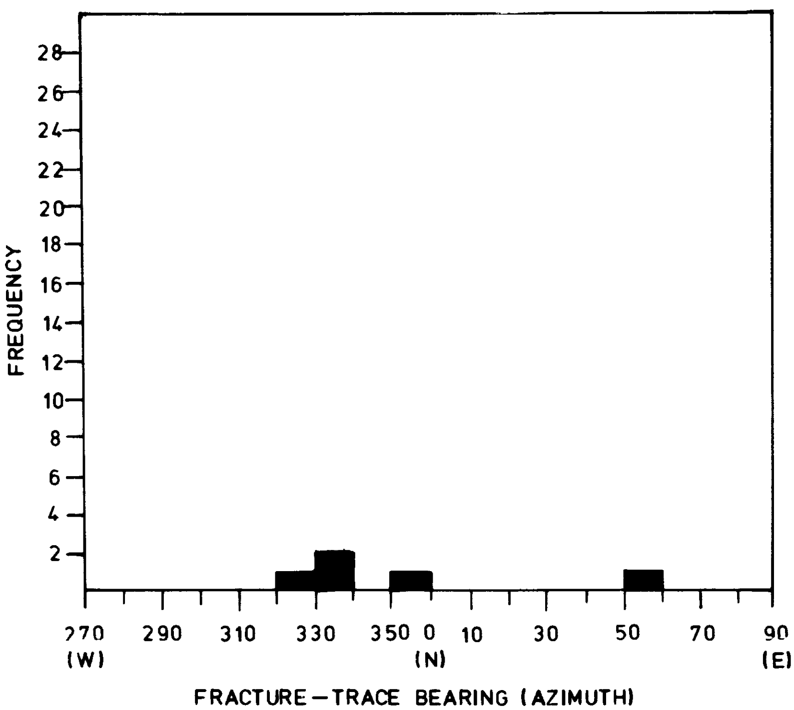

Azimuth Frequency Distribution

Air—photo station 43

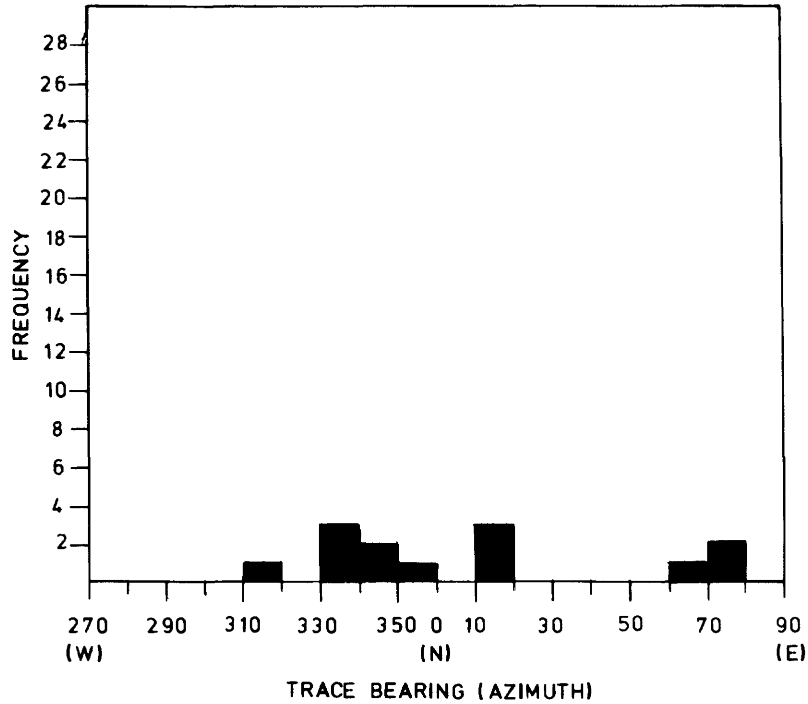

Field station 43

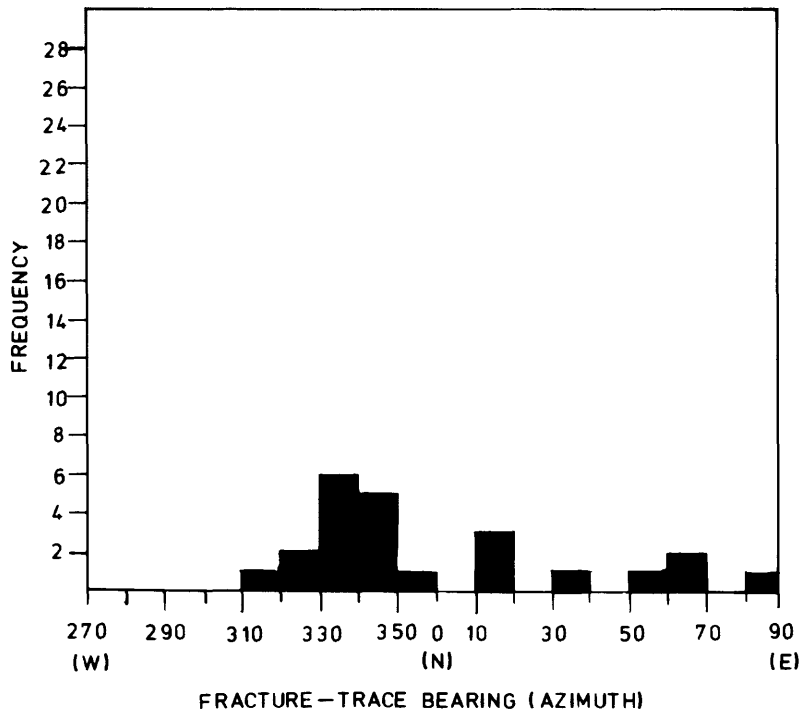

Azimuth Frequency Distribution

Air—photo station 44

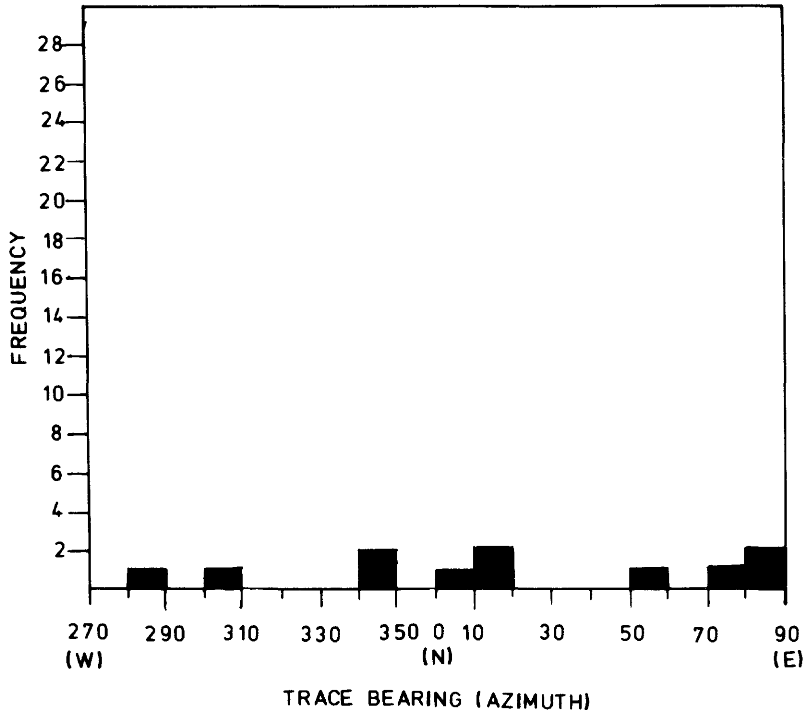

Field station 44

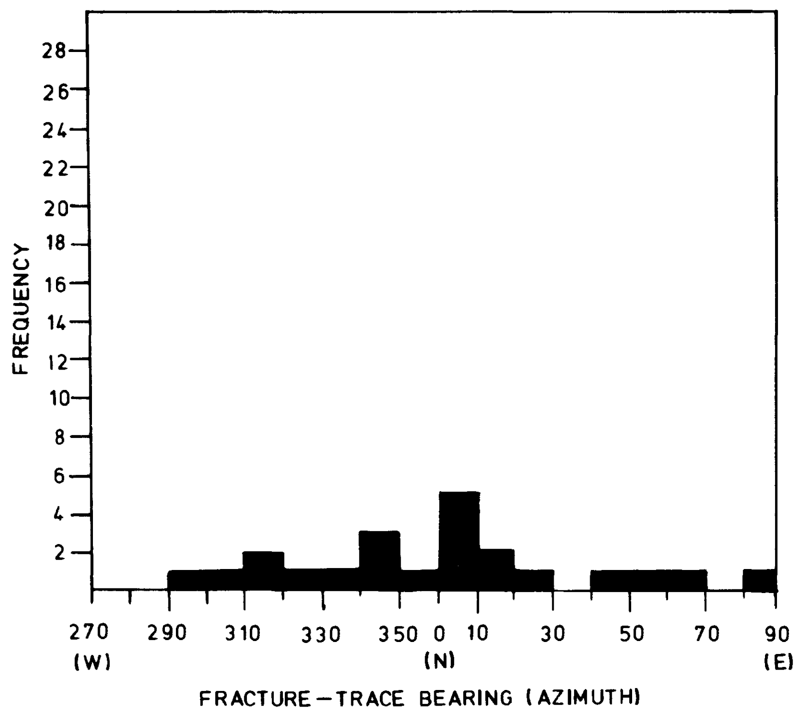

Azimuth Frequency Distribution

Air—photo station 46

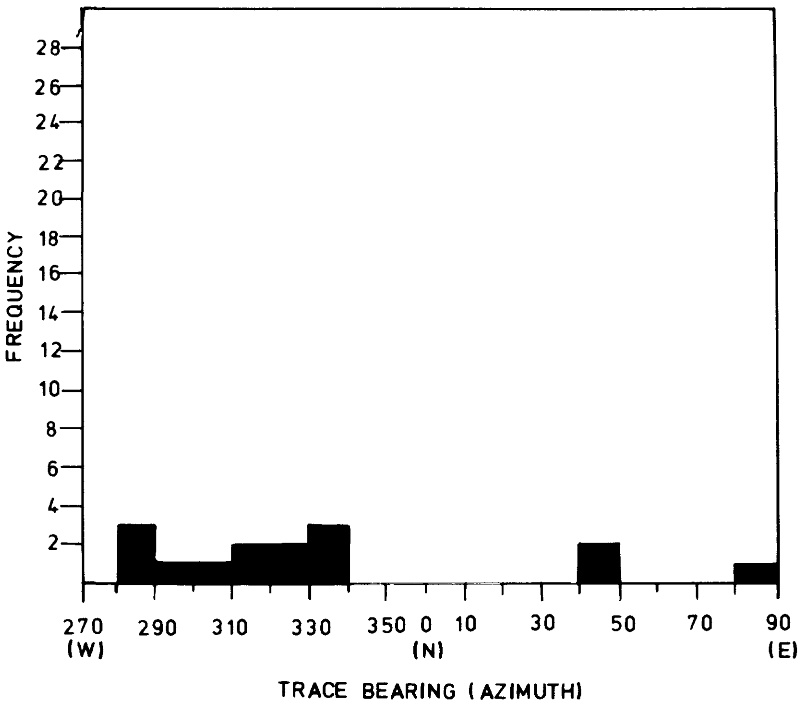

Field station 46

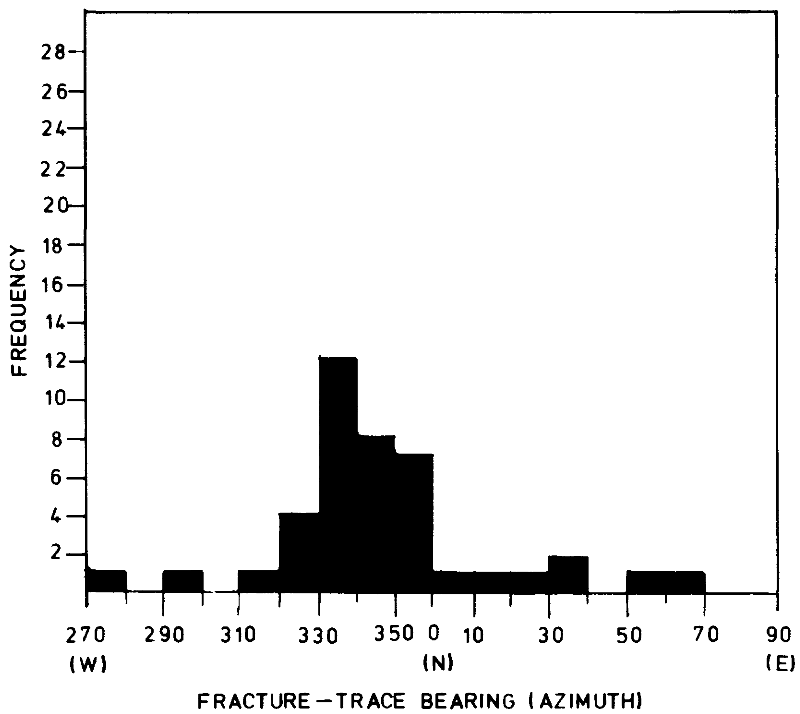

Azimuth Frequency Distribution

Air–photo station 52